Cell Reports

Report

# MOXI Is a Mitochondrial Micropeptide That Enhances Fatty Acid β-Oxidation

## Graphical Abstract

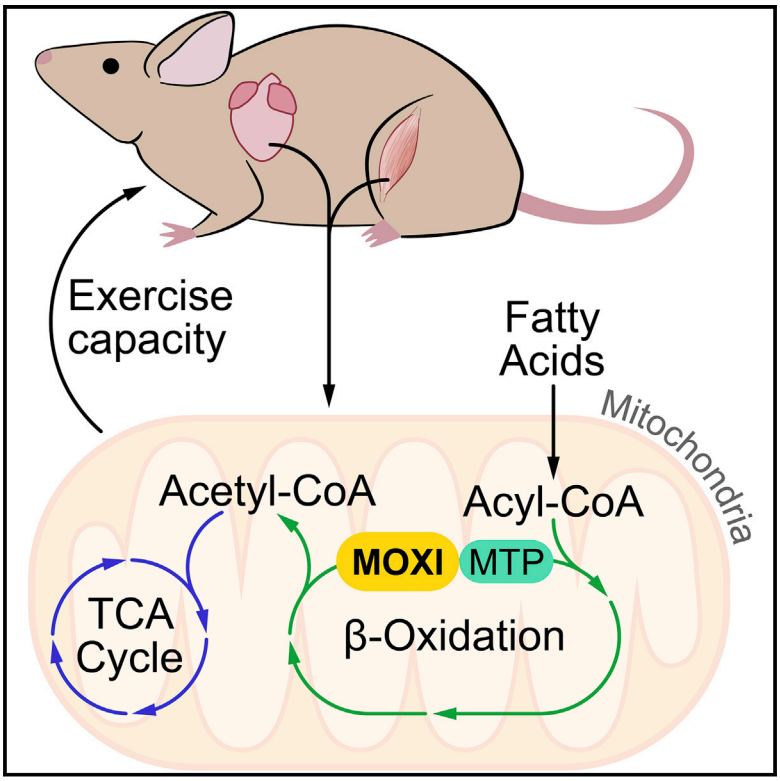


## Authors

Catherine A. Makarewich, Kedryn K. Baskin, Amir Z. Munir, ..., Luke I. Szweda, Rhonda Bassel-Duby, Eric N. Olson

## Correspondence

eric.olson@utsouthwestern.edu

## In Brief

Micropeptide regulator of β-oxidation (MOXI) is encoded by a muscle-enriched RNA transcript misannotated as non-coding. MOXI localizes to the inner mitochondrial membrane where it interacts with the trifunctional protein to modulate fatty acid β-oxidation and exercise capacity.

## Highlights

- MOXI is a muscle-enriched protein encoded by an RNA that is annotated as non-coding
- MOXI interacts with the mitochondrial trifunctional protein and enhances β-oxidation
- MOXI loss- or gain-of-function in mice alters β-oxidation and substrate utilization
- MOXI knockout mice exhibit a reduced capacity for exercise

Makarewich et al., 2018, Cell Reports *23*, 3701–3709
June 26, 2018 
https://doi.org/10.1016/j.celrep.2018.05.058

CellPress

Cell Reports
Report



# MOXI Is a Mitochondrial Micropeptide That Enhances Fatty Acid β-Oxidation

Catherine A. Makarewich,[1] Kedryn K. Baskin,[1] Amir Z. Munir,[1] Svetlana Bezprozvannaya,[1] Gaurav Sharma,[2] Chalermchai Khemtong,[2] Akansha M. Shah,[1] John R. McAnally,[1] Craig R. Malloy,[2,3,4] Luke I. Szweda,[4] Rhonda Bassel-Duby,[1] and Eric N. Olson[1,5,*]

[1]Department of Molecular Biology and the Hamon Center for Regenerative Science and Medicine, University of Texas Southwestern Medical Center, Dallas, TX 75390, USA
[2]Advanced Imaging Research Center, University of Texas Southwestern Medical Center, Dallas, TX 75390, USA
[3]Department of Radiology, University of Texas Southwestern Medical Center, Dallas, TX 75390, USA
[4]Department of Internal Medicine, University of Texas Southwestern Medical Center, Dallas, TX 75390, USA
[5]Lead Contact
*Correspondence: eric.olson@utsouthwestern.edu
https://doi.org/10.1016/j.celrep.2018.05.058

## SUMMARY

**Micropeptide regulator of β-oxidation (MOXI) is a conserved muscle-enriched protein encoded by an RNA transcript misannotated as non-coding. MOXI localizes to the inner mitochondrial membrane where it associates with the mitochondrial trifunctional protein, an enzyme complex that plays a critical role in fatty acid β-oxidation. Isolated heart and skeletal muscle mitochondria from MOXI knockout mice exhibit a diminished ability to metabolize fatty acids, while transgenic MOXI overexpression leads to enhanced β-oxidation. Additionally, hearts from MOXI knockout mice preferentially oxidize carbohydrates over fatty acids in an isolated perfused heart system compared to wild-type (WT) animals. MOXI knockout mice also exhibit a profound reduction in exercise capacity, highlighting the role of MOXI in metabolic control. The functional characterization of MOXI provides insight into the regulation of mitochondrial metabolism and energy homeostasis and underscores the regulatory potential of additional micropeptides that have yet to be identified.**

## INTRODUCTION

Advances in computational biology, transcriptome analyses, and proteomic approaches have revealed that a much larger fraction of the genome is transcribed and translated than initially recognized (Guttman et al., 2009; Ingolia et al., 2014). Notably, many small open reading frames (ORFs) that code for functional protein products have been found hidden within transcripts misannotated as non-coding (Andrews and Rothnagel, 2014; Frith et al., 2006; Mackowiak et al., 2015; Makarewich and Olson, 2017). These small proteins, or micropeptides, play essential roles in diverse biological processes, including development (Chng et al., 2013; Galindo et al., 2007; Kondo et al., 2010), DNA repair (Slavoff et al., 2014), calcium homeostasis (Anderson et al., 2015; Anderson et al., 2016; Magny et al., 2013; Nelson et al., 2016), myoblast fusion (Bi et al., 2017), and metabolism (Lee et al., 2015).

Here, we detail our discovery and analysis of a muscle-enriched protein we termed micropeptide regulator of β-oxidation (MOXI). MOXI is a nuclear encoded peptide that localizes to the inner mitochondrial membrane (IMM), where it specifically interacts with the mitochondrial trifunctional protein (MTP), an IMM localized enzymatic complex that catalyzes the last three steps of long-chain fatty acid (LCFA) oxidation. Mitochondrial fatty acid oxidation is critical for energy homeostasis in skeletal muscle and the heart, and while the major enzymes involved in fatty acid oxidation have been identified, it is still largely unknown how these enzymes are dynamically regulated on a molecular level (Bartlett and Eaton, 2004; Lopaschuk et al., 2010; Nakamura et al., 2014; Rasmussen and Wolfe, 1999; Taegtmeyer et al., 2016). In this regard, our findings indicate that MOXI may fulfill one such role as a regulator of the MTP that helps match the metabolic demand for enhanced fatty acid oxidation in striated muscle during stress conditions.

## RESULTS

### MOXI Is a Conserved Muscle-Enriched Micropeptide

We discovered MOXI through a screen for putative micropeptides encoded by muscle-enriched transcripts annotated as non-coding using PhyloCSF, a comparative genomics method that identifies the evolutionarily conserved protein coding potential of genomic sequences (Lin et al., 2011). This method revealed a previously unrecognized ORF of 56 amino acids within the muscle-enriched *Moxi* transcript, annotated as *1500011K16Rik* and *LINC00116* in the mouse and human genomes, respectively. The murine *Moxi* transcript is encoded in two exons on chromosome 2 and the entire 168 base pair ORF is contained within the first exon (Figures S1A and S1B). The ORF is highly conserved across species (Figure 1A) and scores positively with PhyloCSF (Figure S1A). The N terminus of the MOXI protein is hydrophobic and is predicted to encode a transmembrane domain, whereas the C-terminal region is highly enriched in basic residues (Figure 1A).

To determine if the *Moxi* ORF is translated to a stable micropeptide, we performed *in vitro* transcription and translation

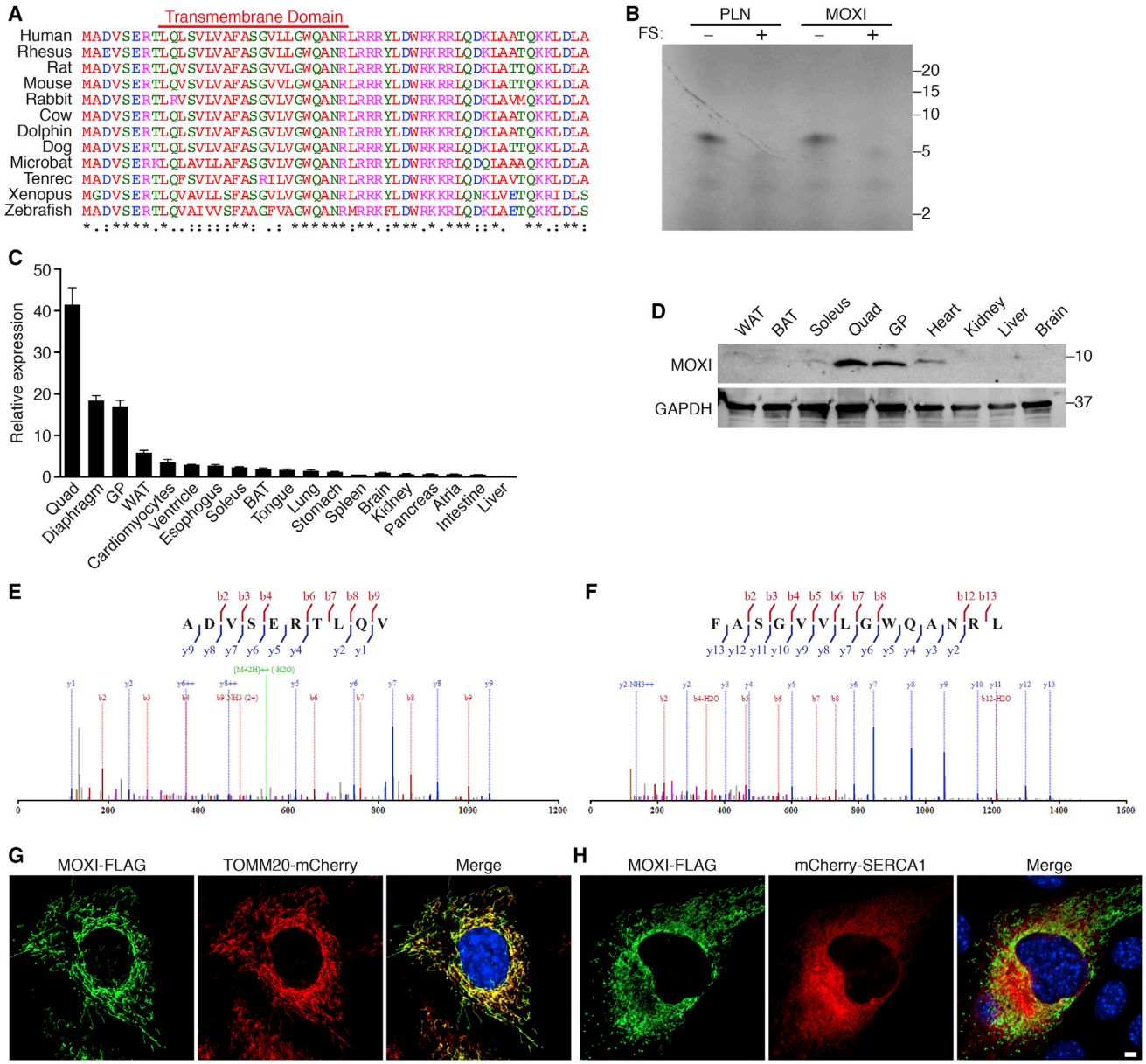


**Figure 1. MOXI Is an Evolutionarily Conserved Micropeptide That Is Enriched in Muscle and Localizes to the Mitochondria**

(A) Amino acid sequence alignment of vertebrate MOXI proteins. The colors of the amino acid residues indicate their properties (pink, positive charge; blue, negative charge; red, hydrophobic; green, hydrophilic). The symbols below the alignment represent the biochemical similarity of aligned amino acids with asterisks indicating identical conservation, colons representing high similarity, and periods showing somewhat similar conservation.

(B) *In vitro* transcription and translation of the full-length *Moxi* or *Pln* RNAs in the presence of radiolabeled $^{35}$S-methionine. Frameshift (FS) mutations introduced within the *Moxi* and *Pln* open reading frames abolished micropeptide expression from these RNAs.

(C) Detection of *Moxi* RNA by qRT-PCR in adult mouse tissues. Quad, quadriceps; GP, gastrocnemius/plantaris; WAT, white adipose tissue; BAT, brown adipose tissue. 18S rRNA was used for normalization and expression is shown relative to liver for n = 3 mice, mean ± SD.

(D) Western blot of adult mouse tissues with a MOXI-specific antibody reveals a band at the predicted size of ~6 kDa.

(E and F) MS/MS spectrum of two unique peptides corresponding to different regions of the MOXI protein identified by mass spectrometry on adult mouse quadriceps muscle.

(G and H) Immunofluorescence of MOXI-FLAG (green) and markers of the mitochondria (TOMM20-mCherry, red) (G) or the sarco/endoplasmic reticulum (mCherry-SERCA1, red) (H) in transfected C2C12 myoblasts. Scale bar, 5 μm.

assays using the full-length *Moxi* RNA transcript in the presence of $^{35}$S-methionine (Figure 1B). A single ~6 kilodalton (kDa) micropeptide was produced from the *Moxi* transcript, whereas a frameshift mutation that disrupted the ORF abolished any detectable expression (Figure 1B). This pattern was identical to that of phospholamban (PLN), a similarly sized 52 amino acid

protein. Quantitative reverse transcription polymerase chain reaction (qRT-PCR) analysis revealed that *Moxi* RNA is highly abundant and enriched in striated muscle (Figure 1C). To further confirm that the *Moxi* transcript encodes a protein and validate its tissue distribution profile, we raised a polyclonal rabbit antibody against MOXI (Figure S1C). Western blot analysis confirmed that MOXI is strongly expressed in both skeletal muscle and the heart (Figure 1D). MOXI was also identified in adult mouse quadriceps muscle by mass spectrometry using in-gel elastase digestion, which produced two distinct peptide fragments of 1.1 and 1.4 kDa that correspond to unique regions of the protein (Figures 1E and 1F).

## MOXI Localizes to the Inner Mitochondrial Membrane

Expression of MOXI as a C-terminal FLAG-fusion protein in C2C12 myoblasts revealed a mitochondrial distribution pattern by immunohistochemistry (Figures 1G and 1H). Co-expression of MOXI-FLAG with an mCherry-tagged mitochondrial membrane marker, translocase of outer mitochondrial membrane 20 (TOMM20), confirmed its mitochondrial localization (Figure 1G). In contrast, co-expression with the endoplasmic reticulum membrane protein sarco/endoplasmic reticulum calcium ATPase (SERCA) revealed distinct and non-overlapping patterns (Figure 1H).

MOXI contains a conserved transmembrane domain comprised of a hydrophobic core that is flanked on both sides by charged amino acid residues (Figure 1A), consistent with sequence determinants of an IMM protein (Stuart and Neupert, 1996). To assess mitochondrial membrane localization, mitochondria were isolated from adult mouse quadriceps muscle and subjected to progressive proteolysis with serial dilutions of proteinase K (PK) (Figure 2A). The outer mitochondrial membrane (OMM) protein TOMM20 was sensitive to proteolysis at much lower PK concentrations than the IMM localized α-subunit of the MTP (HADHA). Similar to HADHA, MOXI was resistant to PK proteolysis at high concentrations of PK and exhibited a degradation pattern consistent with that of an IMM protein (Figure 2A). To further validate its localization to the IMM, mitochondria from quadriceps muscle were subjected to osmotic shock to disrupt the OMM and create mitoplast fractions, which were exposed to PK proteolysis in the presence or absence of detergent (Figure 2B). MOXI exhibited a PK proteolysis resistance pattern similar to that of the IMM marker HADHA, and distinct from the OMM protein TOMM20 (Figure 2B), thus substantiating the sub-mitochondrial localization of MOXI to the IMM.

## MOXI Interacts with the Mitochondrial Trifunctional Protein

To identify protein interaction partners of MOXI, we generated a transgenic (TG) mouse line with striated muscle-specific overexpression of a MOXI-FLAG fusion protein under control of the muscle creatine kinase (MCK) promoter. Proper IMM localization of MOXI-FLAG was validated before immunoprecipitation (IP) experiments were performed (Figures S2A–S2D). Quadriceps muscles of wild-type (WT) and TG mice were homogenized, and lysates were subjected to FLAG IP. Analysis of FLAG-eluted proteins by silver stain revealed three highly abundant proteins that were only present in TG samples (Figure 2C). These unique protein bands were excised and subjected to LC-MS/MS, and peptide mass fingerprinting revealed their identity as MOXI-FLAG and the two subunits of the MTP, the α- (HADHA) and β-subunits (HADHB) (Figure 2C and Tables S1–S3). These results were validated in quadriceps tissue from WT and MOXI-FLAG TG mice by FLAG IP and western blot analysis for HADHA and HADHB (Figure 2D). The interaction of MOXI with the MTP appeared to be specific, as components of the oxidative phosphorylation (OXPHOS) complex, which are highly abundant IMM resident proteins, were excluded from the FLAG elution (Figure 2D). These results were further confirmed in gastrocnemius/plantaris muscles and in the heart of MOXI-FLAG TG mice (Figures S2E and S2F). Additionally, the interaction of MOXI and MTP was confirmed in HEK293 cells transfected with epitope-tagged versions of MOXI (HA), HADHA (Myc), and HADHB (FLAG) (Figure 2E). Cell lysates were subjected to FLAG IP, and bound proteins were eluted using FLAG peptide to purify HADHB-FLAG and its interacting partners. Western blot analysis revealed a strong association of HADHB with both endogenous untagged HADHA and transfected Myc-HADHA (Figure 2E), indicating efficient pull-down of the MTP complex. MOXI-HA was also pulled down in strong association with the MTP, while HA-DWORF, a negative control micropeptide, was not observed in the bound fraction, indicating a specific interaction between MOXI and the MTP (Figure 2E). As the MTP is a critical IMM associated protein that is essential for mitochondrial oxidation of LCFAs, we hypothesized that MOXI plays a role in regulating fatty acid oxidation.

## MOXI Knockout and Transgenic Mice Exhibit Mitochondrial Abnormalities

To assess the function of MOXI *in vivo*, we generated a loss-of-function mouse model by using the clustered regularly interspaced short palindromic repeats (CRISPR)-associated protein 9 (Cas9) system to disrupt the coding frame of *Moxi*. A founder with a 1-base pair deletion and 3-base pair insertion that disrupts the ORF, resulting in premature stop codon and an unstable protein, was chosen for further analysis (Figures S3A and S3B). Heterozygous *Moxi* knockout (KO) mice yielded homozygous mutant offspring at expected Mendelian ratios. Western blot analysis of quadriceps and heart muscle performed with our MOXI-specific antibody showed that the MOXI protein was eliminated in muscle tissues of homozygous mutant KO mice (Figures 3A and 3B). Levels of MOXI overexpression in MOXI TG mice were also assessed by both western blot analysis and qRT-PCR and indicated a high level of expression of the MOXI-FLAG fusion protein, as well as an unanticipated upregulation of the endogenous MOXI protein (Figures 3A–3B and S3C–S3D). It has been demonstrated that mutations in either HADHA or HADHB can result in instability of the MTP complex and reductions in subunit expression levels (Spiekerkoetter et al., 2004a; Ushikubo et al., 1996). Therefore, we assessed whether loss of MOXI protein or its overexpression affected MTP abundance and found no changes in protein or mRNA expression levels of the α- or β-subunits (Figures 3A-3B and S3C–S3D), indicating that MOXI is not required for MTP complex formation or stability.

Compared to WT mice, both KO and TG animals had normal heart function and cardiac dimensions as assessed by

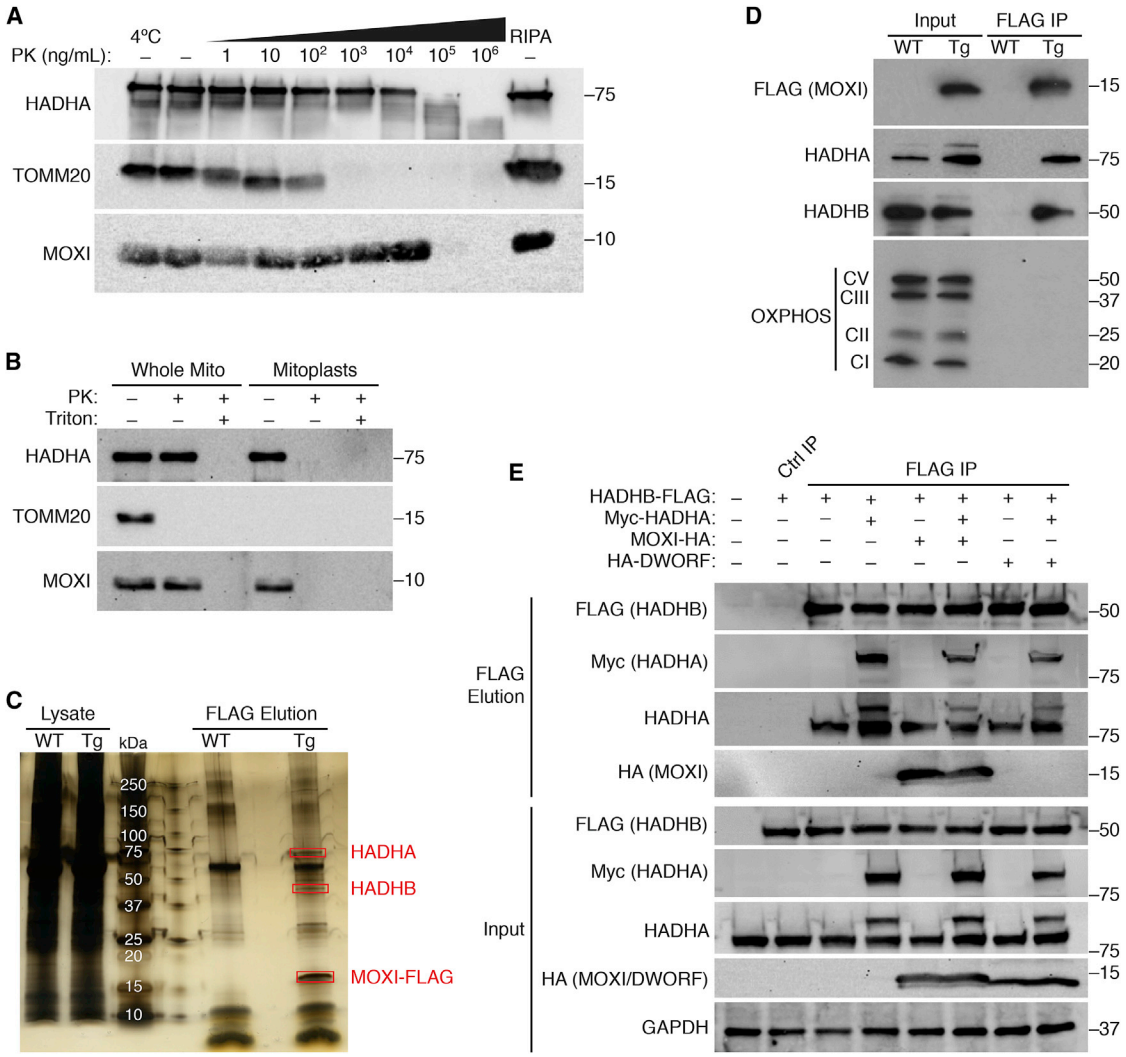


**Figure 2. MOXI Localizes to the Inner Mitochondrial Membrane Where It Interacts with the Mitochondrial Trifunctional Protein**

(A) Mitochondria were isolated from adult mouse quadriceps muscle and subjected to proteinase K (PK) digestion at the indicated concentrations at 37°C unless otherwise indicated. Far right, mitochondria lysed in RIPA buffer serves as a control for the total mitochondrial fraction. Western blots were performed for markers of the OMM (TOMM20), IMM (HADHA), or endogenous MOXI protein.

(B) Mouse quadriceps mitochondria were subjected to PK proteolysis to digest exposed proteins in the presence or absence of detergent (Triton). Osmotic shock was used to isolate mitoplasts, which were also subjected to PK digestion. Western blot analysis was performed using antibodies for MOXI or for the sub-mitochondrial markers HADHA and TOMM20.

(C) Silver stain analysis of FLAG immunoprecipitations (IPs) performed in mouse quadriceps muscle homogenates from wild-type (WT) or MCK-MOXI-FLAG transgenic (TG) mice. The 3 highly abundant and unique bands that are only present in the TG sample and indicated in red rectangles were analyzed by LC-MS/MS and identified as HADHA, HADHB, and MOXI-FLAG (see Tables S1–S3).

(D) Western blot analysis of FLAG IPs from quadriceps muscle homogenates of WT and MOXI-FLAG TG mice using antibodies for HADHA, HADHB, FLAG, and an OXPHOS cocktail that detects Complex I, II, III, and V of the OXPHOS complex.

(E) Co-immunoprecipitation (coIP) experiments in transfected HEK293 cells using HADHB-FLAG, Myc-HADHA and MOXI-HA or HA-DWORF. Cell lysates were immunoprecipitated using FLAG magnetic beads or a control IgG resin, and bound proteins were eluted using FLAG peptide. Proteins that were pulled down in association with HADHB-FLAG were analyzed by western blot analysis using antibodies for FLAG, Myc, HADHA, or HA. Ctrl IP, control immunoprecipitation. The HADHA antibody recognizes both the endogenous protein (lower molecular weight band) and the transfected Myc-HADHA protein (higher molecular weight band).

echocardiography (Figures S3E–S3H) and all genotypes had comparable body composition measured by EchoMRI (Figures S3I–S3K). Histologically, quadriceps sections from KO mice appeared normal, while TG animals exhibited signs of myopathy with many fibers containing centralized nuclei (Figure 3C). Additionally, degenerating muscle fibers were present throughout skeletal muscle sections of TG mice, indicating severe pathology (Figure 3C). Immunohistochemistry performed on quadriceps sections showed an accumulation of desmin in skeletal muscle fibers of TG animals, demonstrating a loss of membrane integrity

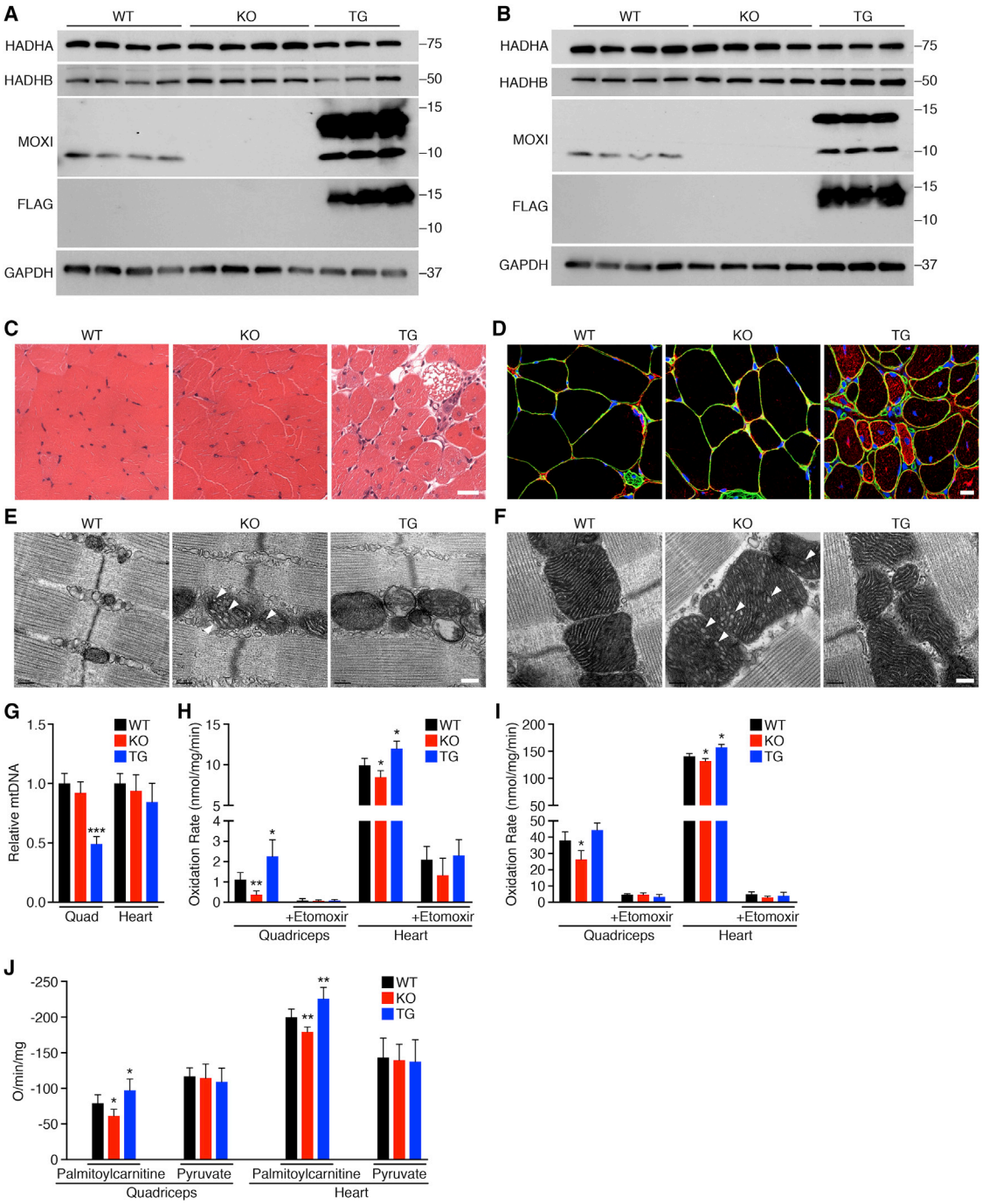


**Figure 3. Consequence of MOXI Loss- and Gain-of-Function**

(A and B) Western blot analysis showing the expression level of MOXI in quadriceps muscle (A) and heart (B) of WT, KO, and TG mice. The expression and stability of the MTP α-subunit (HADHA) and β-subunit (HADHB) were also analyzed.

(C) Hematoxylin and eosin (H&E) staining on quadriceps muscle sections. Scale bar, 50 μm.

(D) Immunohistochemistry on quadriceps muscle sections. Representative merged images are shown of laminin (green), desmin (red), and DAPI (blue). Scale bar, 10 μm.

(E and F) Transmission electron micrographs of quadriceps muscle (E) and heart (F) from WT, KO, and TG mice. White arrows indicate the disrupted cristae structure observed in KO mice. Representative images from n = 3 mice are shown. Scale bar, 0.2 μm.

(G) Relative mitochondrial DNA (mtDNA) content expressed as a function of total genomic DNA in quadriceps (Quad) and hearts of WT, KO, and TG mice. Data were acquired by qPCR and are represented as mean ± SD, n = 5 mice per genotype, $^{**}p < 0.005$.

*(legend continued on next page)*

(Figure 3D). Succinate dehydrogenase (SDH) staining of quadriceps muscles from WT, KO, and TG mice revealed no overt differences in relative oxidative capacity among genotypes (Figure S4A); however, TG muscle fibers presented with a ragged appearance, suggesting mitochondrial abnormalities.

We assessed the ultrastructure of quadriceps muscle and heart from WT, KO, and TG mice by electron microscopy (EM) and observed unique mitochondrial abnormalities in KO and TG mice (Figures 3E–3F and S4B–S4C). KO mitochondria presented with an enlarged appearance with swollen and disrupted cristae structure in both quadriceps muscle (Figures 3E and S4B) and heart (Figures 3F and S4C). These features are consistent with previous reports from heterozygous *HADHA*$^{+/-}$ mice that present with similar mitochondrial abnormalities (Ibdah et al., 2005; Rector et al., 2008). Additionally, EM images from TG mice reveal a clear disorganization of the mitochondrial network with regions of mitochondrial dropout that are most clearly seen in quadriceps muscle (Figures 3E and S4B) and are also present in heart sections (Figures 3F and S4C). Mitochondrial content of quadriceps and heart from WT, KO, and TG mice were assayed by mitochondrial DNA (mtDNA) content and revealed no significant difference between WT and KO animals in either tissue; however, there was a significant reduction in mtDNA content in TG quadriceps muscle (Figure 3G) that correlated with the mitochondrial dropout seen by EM in these animals (Figures 3E and S4B).

## MOXI Loss-or Gain-of-Function in Mice Alters Fatty Acid β-Oxidation

To directly measure the effect of MOXI gene deletion or overexpression on LCFA oxidation, *ex vivo* palmitate oxidation was measured in isolated skeletal muscle and heart mitochondria from WT, KO, and TG mice by assessing the rate of conversion of radiolabeled palmitate into either $CO_2$ (Figure 3H) or acid-soluble metabolites (Figure 3I). Isolated quadriceps and heart mitochondria from KO mice exhibited a diminished ability to metabolize LCFAs compared to WT mice (Figures 3H and 3I), indicating that muscles from these animals have a lower fatty acid oxidation capacity, while TG mitochondria showed enhanced oxidation. There were no observable differences in oxidation rates in the presence of etomoxir, a potent carnitine palmitoyltransferase I (CPT-1) inhibitor, indicating similar levels of contributing non-mitochondrial oxidation between genotypes (Figures 3H and 3I).

To further assess mitochondrial function in our animals, we analyzed ADP-stimulated respiration in isolated mitochondria from quadriceps and heart tissue using either LCFAs (palmitoylcarnitine) or pyruvate as the oxidative substrate. A significant reduction in the rate of state 3 respiration was observed in mitochondria isolated from both quadriceps and heart tissues of KO mice when palmitoylcarnitine was provided as the substrate, while no change was seen when pyruvate oxidation was assessed (Figure 3J), indicating that respiratory function is selectively impaired for fatty acid oxidation. Conversely, palmitoylcarnitine oxidation was selectively enhanced in both skeletal muscle and heart mitochondria from TG mice, while pyruvate oxidation was unchanged (Figure 3J), once again highlighting the substrate-specific effect of MOXI overexpression on mitochondrial respiratory function.

## MOXI Loss-of-Function Leads to Reduced LCFA β-Oxidation and an Intolerance to Exercise

To determine the effect of MOXI loss-of-function on substrate utilization in the heart, substrate oxidation was evaluated using $^{13}$C-NMR isotopomer analysis in isolated perfused WT and KO heart preparations. TG mice were omitted from these studies due to the severe mitochondrial phenotype exhibited by these animals. Figure S4D shows the metabolism of $^{13}$C-enriched substrates provided in the cardiac perfusate. Multiplet ratios in glutamate were analyzed in isolated hearts for the metabolism of [1,6-$^{13}C_2$]glucose, [3-$^{13}$C]lactate, [3-$^{13}$C]pyruvate, and [U-$^{13}$C]LCFA supplied during perfusion (Figure S4D). In this study, the labeling pattern does not allow distinction between glucose, pyruvate, and lactate oxidation, and for this reason, they are collectively termed carbohydrates. The $^{13}$C multiplets from glutamate C-2 (Figure 4A), C-4 (Figure 4B), and C-3 (Figure 4C) were analyzed to evaluate substrate oxidation. KO hearts showed a decrease in C-3 and C-4 doublets with a corresponding increase in the C-2 doublet of glutamate (Figures 4A–C). $^{13}$C-NMR isotopomer analysis of heart extracts from KO mice showed a decrease in LCFA oxidation and a corresponding increase in carbohydrate oxidation compared to WT hearts (Figures 4D and 4E), demonstrating that KO hearts oxidized significantly more carbohydrates than fatty acids for energy production (Figure 4E). TCA cycle flux (Figure 4F), coronary flow rate (Figure S4E), and oxygen consumption rate (Figure S4F) measured under the metabolic steady state were not significantly different between groups. Consistent with our previous results showing that mitochondria from MOXI KO mice have an impaired fatty acid oxidation capacity, these data show that functioning hearts from KO mice preferentially oxidize carbohydrates over fatty acids as substrates.

β-oxidation is a key metabolic pathway for energy homeostasis during physiological stresses such as exercise when glucose supply becomes limited and several fatty acid oxidation disorders are associated with exercise intolerance (Rinaldo et al., 2002; Spiekerkoetter et al., 2004b; Spiekerkoetter et al., 2005; Spiekerkoetter and Wood, 2010). Therefore, we examined the response of MOXI KO mice to forced treadmill running to assess their ability to respond to physical exercise. KO mice showed a significant reduction in exercise capacity as compared to WT mice and exhibited signs of exhaustion after running only half the distance and time of WT mice (Figures 4G and 4H). WT

(H and I) Fatty acid oxidation was measured by incubation of quadriceps or heart mitochondria from WT, KO, and TG mice with [$^{14}$C]-palmitate. Oxidation rates were determined by analyzing captured $CO_2$ (H) and acid soluble metabolites (ASM) (I). Where indicated, the CPT-1 inhibitor etomoxir (40 μM) was used. Data are represented as mean ± SD, n = 8 for WT and KO and n = 6 for TG. *p < 0.05, **p < 0.01.

(J) Oxygen (O) consumption rates were measured in isolated mitochondria from WT, KO, and TG mice using 1 mM malate and either palmitoylcarnitine (25 μM for heart, 50 μM for quad) or pyruvate (100 μM) as metabolic substrates. State 3 respiration was initiated with the addition of ADP at a final concentration of 0.25 mM. Data are presented as mean ± SD, n = 6 per genotype. *p < 0.05, **p < 0.01.

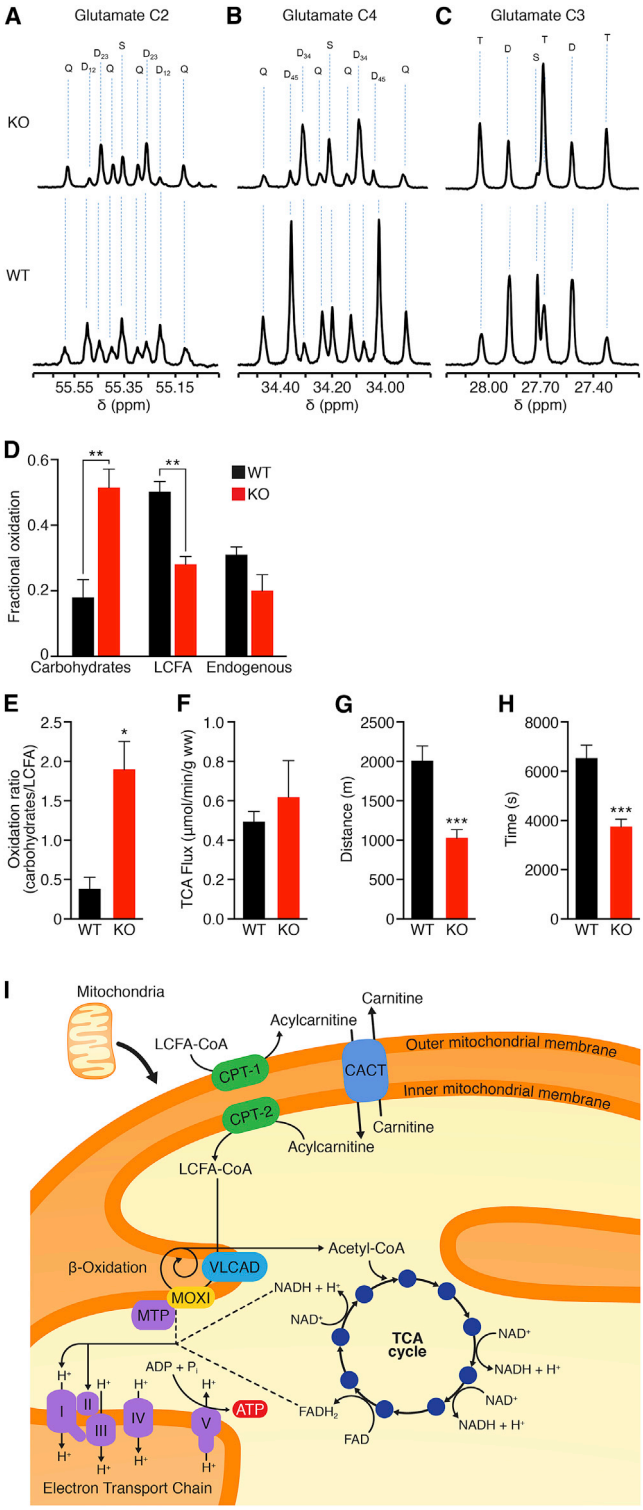


**Figure 4. $^{13}$C-NMR Isotopomer Analysis in WT and KO Hearts and Response of KO Mice to Exercise**

(A–F) Substrate oxidation was evaluated using $^{13}$C-NMR isotopomer analysis in isolated hearts from WT and KO mice perfused with $^{13}$C-labeled LCFA and carbohydrate substrates. Glutamate C-2 (55.35 ppm) (A), C-4 (34.20 ppm) (B), and C-3 (27.60 ppm) (C) spectra. The letters S, D, T, and Q refer to a singlet, doublet (with the relevant J-coupled spins), triplet (a degenerate doublet of doublets), or Q (quartet or doublet of doublets). Fractional oxidation (D), carbohydrate to long-chain fatty acid oxidation ratio (E), and TCA flux (F) were assessed for n = 4 mice per genotype. Data are presented as mean ± SEM with significance indicated as *p < 0.05, **p < 0.01.

(G and H) Exercise capacity was measured using forced treadmill running to exhaustion. MOXI KO mice ran ~49% less distance (G) and time (H) than WT littermate controls (n = 14). Data are represented as mean ± SD ***p < 0.005.

(I) Working model for MOXI function. LCFAs are converted from acyl-CoA molecules into acylcarnitines by carnitine palmitoyltransferase 1 (CPT-1) and shuttled across the mitochondrial membrane by the carnitine-acylcarnitine translocase (CACT) where they are converted back to LCFA-CoA molecules by carnitine palmitoyltransferase 2 (CPT-2). LCFA-CoAs are metabolized by the inner membrane bound enzymes very long chain acyl-CoA dehydrogenase (VLCAD) and the mitochondrial trifunctional protein (MTP)/MOXI complex to generate acetyl-CoA molecules that then enter the TCA cycle for production of ATP and reducing coenzymes such as NADH and $FADH_2$. These reducing coenzymes can then be utilized by the electron transport chain to produce additional ATP.

and KO mice did not lose significant weight during this acute bout of exercise, and there were no differences in blood lactate levels between groups before or after exercise (Figures S4G and S4H). These results further underscore the important role of MOXI in fatty acid oxidation and its requirement for maintaining energy homeostasis during increased metabolic demand (Figure 4I).

## DISCUSSION

Fatty acids are a major fuel source required to sustain contractile function in skeletal muscle and the heart, and while the major enzymes involved in β-oxidation have been identified, the precise manner in which they are regulated is still unknown (Bartlett and Eaton, 2004; Lopaschuk et al., 2010; Nakamura et al., 2014; Rasmussen and Wolfe, 1999; Taegtmeyer et al., 2016). Here, we identify MOXI as a muscle-enriched micropeptide that interacts with the MTP in the mitochondrial inner membrane and enhances fatty acid oxidation (Figure 4I), which is required to convert the energy stored in fats into ATP. The importance of MOXI as a regulator of fatty acid oxidation is demonstrated in our loss-of-function studies where hearts from MOXI KO mice switch from using fatty acids to carbohydrates as their preferred substrate (Figures 4A–4E). The discovery of MOXI as a micropeptide capable of enhancing fatty acid oxidation through its interaction with the MTP provides insights into the complex process of metabolic control and suggests that the enzyme complexes involved in β-oxidation may be regulated by interactions with small regulatory proteins that have yet to be discovered.

In humans, fatty acid oxidation disorders present as a variety of clinical phenotypes and can result in severe disease during the early stages of life due to limited glycogen stores and a high metabolic rate that relies heavily on fatty acid oxidation for energy (Nsiah-Sefaa and McKenzie, 2016). In late-onset β-oxidation disease, symptoms can include skeletal muscle myopathies and exercise intolerance, cardiovascular disease, and neuropathy (Kompare and Rizzo, 2008). Depending on the gene affected and the exact mutation observed, the severity of fatty acid oxidation disorders varies immensely. Similar to several other gene mutations linked to β-oxidation disorders

(Cox et al., 2001; Spiekerkoetter et al., 2004b; Spiekerkoetter et al., 2005; Spiekerkoetter and Wood, 2010), no overt phenotype is observed in a loss-of-function MOXI mouse model at rest; however, when challenged with physiological stress such as exercise, MOXI KO mice fail to maintain metabolic homeostasis. There is still a great deal to be learned about how MOXI exerts its dynamic control on the MTP complex, and elucidating the precise mechanism by which it induces its effect will be the focus of future work.

In summary, the discovery of MOXI highlights the role of a previously overlooked small protein in regulating fatty acid oxidation and metabolic responsiveness. Similar to other recently discovered micropeptides (Anderson et al., 2015; Anderson et al., 2016; Nelson et al., 2016), MOXI appears to exert its biological activity by engaging with and modulating a much larger protein complex. The small size of MOXI and its distinct amino acid sequence likely contribute to its capacity to fine-tune the activity of the MTP and regulate such a complex biological system. Furthermore, our findings underscore the likelihood that additional transcripts currently classified as non-coding are misannotated and contain small ORFs that encode functional proteins. These micropeptides could serve as critical regulators of essential biological processes, and the prospect of identifying these proteins provides exciting opportunites for future discoveries.

## EXPERIMENTAL PROCEDURES

Additional details and resources used in this work can be found in Supplemental Experimental Procedures.

### Animals

All animal work described in this manuscript has been approved and conducted under the oversight of the UT Southwestern Institutional Animal Care and Use Committee. All mouse lines were generated on a pure C57BL/6N background. All functional experiments were performed using 12- to 16-week-old male mice.

### MOXI Antibody Production

A custom polyclonal antibody was derived against the predicted MOXI protein by New England Peptide. Rabbits were immunized with a synthetic peptide with the following sequence: RYLDWRKRRLQDKL. Sera were collected and affinity purified against the peptide immunogen.

### Mitochondrial Isolations for Functional Analysis

Tissues were homogenized in ice cold isolation buffer (10 mM MOPS, 210 mM mannitol, 70 mM sucrose, and 1 mM EDTA, pH 7.4). Mitochondria were resuspended in isolation buffer for mitochondrial respiratory function analysis or STE buffer (250 mM sucrose, 10 mM Tris-HCl, 1 mM EDTA, pH 7.4) for fatty acid oxidation assays. Additional information can be found in Supplemental Experimental Procedures.

### Long-Chain Fatty Acid Oxidation Assays

Isolated mitochondria were incubated in oxidation reaction buffer (100 mM sucrose, 10 mM Tris-HCl, 5 mM $KH_2PO_4$, 0.2 mM EDTA, 80 mM KCl, 1 mM $MgCl_2$, 2 mM L-carnitine, 0.1 mM malate, 0.05 mM coenzyme A, 2 mM ATP, 1 mM DTT, and 0.7% BSA/0.1 mM palmitate/0.4 μCi $^{14}$C-palmitate) for 1 hr then transferred to tubes containing 1 M perchloric acid. Fully oxidized $CO_2$ was captured on Whatman filter paper discs treated with 1 M NaOH and acid-soluble metabolites (ASMs) were analyzed by scintillation counting. Additional details can be found in Supplemental Experimental Procedures.

### Mitochondrial Respiratory Function Analysis

Isolated heart mitochondria were diluted to 0.25 mg/mL (heart) or 0.5 mg/mL (quadriceps) in respiratory buffer composed of 10 mM MOPS, 210 mM mannitol, 70 mM sucrose, and 5 mM $K_2HPO_4$ at pH 7.4 and incubated with the indicated substrates. For measurements with quadriceps mitochondria, 1.25 mM $MgCl_2$ was also included in the respiratory buffer. State 3 respiration was initiated after 2 min with ADP at a final concentration of 0.25 mM. Rates of mitochondrial respiration were evaluated using a Neofox oxygen chamber. Detailed information can be found in Supplemental Experimental Procedures.

### $^{13}$C-NMR Isotopomer Analysis

Hearts were cannulated via aorta and perfused for 30 min at 100 cm $H_2O$ pressure at 37°C with a modified Krebs-Henseleit (KH) buffer containing 8 mM [1,6-$^{13}$C]glucose, 1.2 mM [3-$^{13}$C]lactate, 0.12 mM [3-$^{13}$C]pyruvate, 0.4 mM [U-$^{13}$C]long-chain fatty acids (LCFA), 0.75% bovine serum albumin (BSA), and 2.5 mM $CaCl_2$ equilibrated with 95:5 $O_2$:$CO_2$. After 30 min of perfusion, hearts were snap-frozen in liquid nitrogen. Proton-decoupled $^{13}$C-NMR spectra of heart extracts were acquired at 600 MHz spectrometer (Bruker Corporation, USA) equipped with 5 mm cryoprobe. Additional information can be found in Supplemental Experimental Procedures.

### Treadmill Exercise

Mice were run on Exer-3/6 treadmill apparatus (Columbus Instruments) with mild electrical stimulus. The treadmill was set to ramp from 0 to 10 m/min over a period of 5 min and then stay at 10 m/min for an additional 5 min. The treadmill speed then incrementally increased (1 m/min every 5 min) to a maximum speed of 20 m/min until exhaustion. Exhaustion was defined by failure to run for greater than 10 s.

### Quantification and Statistical Analysis

Statistical comparisons between groups were evaluated by Student's t test using Prism 6 (GraphPad). Data are presented as mean ± SD or SEM as indicated in each figure legend. Statistical significance is denoted as $*p < 0.05$, $**p < 0.01$, $***p < 0.005$, and $****p < 0.001$; n indicates the number of biological replicates within each group.

## SUPPLEMENTAL INFORMATION

Supplemental Information includes Supplemental Experimental Procedures, four figures, and three tables, and can be found with this article online at https://doi.org/10.1016/j.celrep.2018.05.058.

## ACKNOWLEDGMENTS

We thank J. Cabrera for graphics, H. Sadek for scientific discussion and insight, W. Tan for echocardiography, J. Karch for providing protocols and advice, and the following Core Facilities at the University of Texas Southwestern Medical Center: The Molecular Pathology Core under the direction of J. Richardson; the Electron Microscopy Core under the direction of K. Luby-Phelps; and the Proteomics Core under the direction of H. Mirzaei. This work was supported by grants from the NIH (HL-130253, HL-138426, HD-087351, DK-099653, AR-067294, P41-EB015908, and R37-HL034557), American Heart Association (16POST31100009 to K.K.B.), Fondation Leducq Networks of Excellence, and the Robert A. Welch Foundation (grant 1-0025 to E.N.O.). C.A.M. was supported by a National Heart, Lung, and Blood Institute, NIH, Ruth L. Kirschstein National Research Service Award (NRSA) (F32HL129674).

## AUTHOR CONTRIBUTIONS

Conceptualization, C.A.M., K.K.B., A.Z.M., C.R.M., L.I.S., and E.N.O.; Methodology, C.A.M., A.Z.M., K.K.B., S.B., A.M.S., J.R.M., G.S., and C.K.; Visualization, C.A.M., K.K.B., and A.Z.M.; Writing, C.A.M., R.B.D., and E.N.O., Supervision, C.R.M., L.I.S., R.B.D., and E.N.O.; Project Administration, C.A.M. and R.B.D.; Funding Acquisition, C.A.M., K.K.B., C.R.M., L.I.S., R.B.D., and E.N.O.

## DECLARATION OF INTERESTS

The authors declare no competing interests.

Received: January 2, 2018
Revised: April 10, 2018
Accepted: May 16, 2018
Published: June 26, 2018

## REFERENCES

Anderson, D.M., Anderson, K.M., Chang, C.L., Makarewich, C.A., Nelson, B.R., McAnally, J.R., Kasaragod, P., Shelton, J.M., Liou, J., Bassel-Duby, R., and Olson, E.N. (2015). A micropeptide encoded by a putative long noncoding RNA regulates muscle performance. Cell *160*, 595–606.

Anderson, D.M., Makarewich, C.A., Anderson, K.M., Shelton, J.M., Bezprozvannaya, S., Bassel-Duby, R., and Olson, E.N. (2016). Widespread control of calcium signaling by a family of SERCA-inhibiting micropeptides. Sci. Signal. *9*, ra119.

Andrews, S.J., and Rothnagel, J.A. (2014). Emerging evidence for functional peptides encoded by short open reading frames. Nat. Rev. Genet. *15*, 193–204.

Bartlett, K., and Eaton, S. (2004). Mitochondrial beta-oxidation. Eur. J. Biochem. *271*, 462–469.

Bi, P., Ramirez-Martinez, A., Li, H., Cannavino, J., McAnally, J.R., Shelton, J.M., Sánchez-Ortiz, E., Bassel-Duby, R., and Olson, E.N. (2017). Control of muscle formation by the fusogenic micropeptide myomixer. Science *356*, 323–327.

Chng, S.C., Ho, L., Tian, J., and Reversade, B. (2013). ELABELA: a hormone essential for heart development signals via the apelin receptor. Dev. Cell *27*, 672–680.

Cox, K.B., Hamm, D.A., Millington, D.S., Matern, D., Vockley, J., Rinaldo, P., Pinkert, C.A., Rhead, W.J., Lindsey, J.R., and Wood, P.A. (2001). Gestational, pathologic and biochemical differences between very long-chain acyl-CoA dehydrogenase deficiency and long-chain acyl-CoA dehydrogenase deficiency in the mouse. Hum. Mol. Genet. *10*, 2069–2077.

Frith, M.C., Forrest, A.R., Nourbakhsh, E., Pang, K.C., Kai, C., Kawai, J., Carninci, P., Hayashizaki, Y., Bailey, T.L., and Grimmond, S.M. (2006). The abundance of short proteins in the mammalian proteome. PLoS Genet. *2*, e52.

Galindo, M.I., Pueyo, J.I., Fouix, S., Bishop, S.A., and Couso, J.P. (2007). Peptides encoded by short ORFs control development and define a new eukaryotic gene family. PLoS Biol. *5*, e106.

Guttman, M., Amit, I., Garber, M., French, C., Lin, M.F., Feldser, D., Huarte, M., Zuk, O., Carey, B.W., Cassady, J.P., et al. (2009). Chromatin signature reveals over a thousand highly conserved large non-coding RNAs in mammals. Nature *458*, 223–227.

Ibdah, J.A., Perlegas, P., Zhao, Y., Angdisen, J., Borgerink, H., Shadoan, M.K., Wagner, J.D., Matern, D., Rinaldo, P., and Cline, J.M. (2005). Mice heterozygous for a defect in mitochondrial trifunctional protein develop hepatic steatosis and insulin resistance. Gastroenterology *128*, 1381–1390.

Ingolia, N.T., Brar, G.A., Stern-Ginossar, N., Harris, M.S., Talhouarne, G.J., Jackson, S.E., Wills, M.R., and Weissman, J.S. (2014). Ribosome profiling reveals pervasive translation outside of annotated protein-coding genes. Cell Rep. *8*, 1365–1379.

Kompare, M., and Rizzo, W.B. (2008). Mitochondrial fatty-acid oxidation disorders. Semin. Pediatr. Neurol. *15*, 140–149.

Kondo, T., Plaza, S., Zanet, J., Benrabah, E., Valenti, P., Hashimoto, Y., Kobayashi, S., Payre, F., and Kageyama, Y. (2010). Small peptides switch the transcriptional activity of Shavenbaby during Drosophila embryogenesis. Science *329*, 336–339.

Lee, C., Zeng, J., Drew, B.G., Sallam, T., Martin-Montalvo, A., Wan, J., Kim, S.J., Mehta, H., Hevener, A.L., de Cabo, R., and Cohen, P. (2015). The mitochondrial-derived peptide MOTS-c promotes metabolic homeostasis and reduces obesity and insulin resistance. Cell Metab. *21*, 443–454.

Lin, M.F., Jungreis, I., and Kellis, M. (2011). PhyloCSF: a comparative genomics method to distinguish protein coding and non-coding regions. Bioinformatics *27*, i275–i282.

Lopaschuk, G.D., Ussher, J.R., Folmes, C.D., Jaswal, J.S., and Stanley, W.C. (2010). Myocardial fatty acid metabolism in health and disease. Physiol. Rev. *90*, 207–258.

Mackowiak, S.D., Zauber, H., Bielow, C., Thiel, D., Kutz, K., Calviello, L., Mastrobuoni, G., Rajewsky, N., Kempa, S., Selbach, M., and Obermayer, B. (2015). Extensive identification and analysis of conserved small ORFs in animals. Genome Biol. *16*, 179.

Magny, E.G., Pueyo, J.I., Pearl, F.M., Cespedes, M.A., Niven, J.E., Bishop, S.A., and Couso, J.P. (2013). Conserved regulation of cardiac calcium uptake by peptides encoded in small open reading frames. Science *341*, 1116–1120.

Makarewich, C.A., and Olson, E.N. (2017). Mining for Micropeptides. Trends Cell Biol. *27*, 685–696.

Nakamura, M.T., Yudell, B.E., and Loor, J.J. (2014). Regulation of energy metabolism by long-chain fatty acids. Prog. Lipid Res. *53*, 124–144.

Nelson, B.R., Makarewich, C.A., Anderson, D.M., Winders, B.R., Troupes, C.D., Wu, F., Reese, A.L., McAnally, J.R., Chen, X., Kavalali, E.T., et al. (2016). A peptide encoded by a transcript annotated as long noncoding RNA enhances SERCA activity in muscle. Science *351*, 271–275.

Nsiah-Sefaa, A., and McKenzie, M. (2016). Combined defects in oxidative phosphorylation and fatty acid β-oxidation in mitochondrial disease. Biosci. Rep. *36*, e00313.

Rasmussen, B.B., and Wolfe, R.R. (1999). Regulation of fatty acid oxidation in skeletal muscle. Annu. Rev. Nutr. *19*, 463–484.

Rector, R.S., Payne, R.M., and Ibdah, J.A. (2008). Mitochondrial trifunctional protein defects: clinical implications and therapeutic approaches. Adv. Drug Deliv. Rev. *60*, 1488–1496.

Rinaldo, P., Matern, D., and Bennett, M.J. (2002). Fatty acid oxidation disorders. Annu. Rev. Physiol. *64*, 477–502.

Slavoff, S.A., Heo, J., Budnik, B.A., Hanakahi, L.A., and Saghatelian, A. (2014). A human short open reading frame (sORF)-encoded polypeptide that stimulates DNA end joining. J. Biol. Chem. *289*, 10950–10957.

Spiekerkoetter, U., and Wood, P.A. (2010). Mitochondrial fatty acid oxidation disorders: pathophysiological studies in mouse models. J. Inherit. Metab. Dis. *33*, 539–546.

Spiekerkoetter, U., Khuchua, Z., Yue, Z., Bennett, M.J., and Strauss, A.W. (2004a). General mitochondrial trifunctional protein (TFP) deficiency as a result of either alpha- or beta-subunit mutations exhibits similar phenotypes because mutations in either subunit alter TFP complex expression and subunit turnover. Pediatr. Res. *55*, 190–196.

Spiekerkoetter, U., Tokunaga, C., Wendel, U., Mayatepek, E., Exil, V., Duran, M., Wijburg, F.A., Wanders, R.J., and Strauss, A.W. (2004b). Changes in blood carnitine and acylcarnitine profiles of very long-chain acyl-CoA dehydrogenase-deficient mice subjected to stress. Eur. J. Clin. Invest. *34*, 191–196.

Spiekerkoetter, U., Tokunaga, C., Wendel, U., Mayatepek, E., Ijlst, L., Vaz, F.M., van Vlies, N., Overmars, H., Duran, M., Wijburg, F.A., et al. (2005). Tissue carnitine homeostasis in very-long-chain acyl-CoA dehydrogenase-deficient mice. Pediatr. Res. *57*, 760–764.

Stuart, R.A., and Neupert, W. (1996). Topogenesis of inner membrane proteins of mitochondria. Trends Biochem. Sci. *21*, 261–267.

Taegtmeyer, H., Young, M.E., Lopaschuk, G.D., Abel, E.D., Brunengraber, H., Darley-Usmar, V., Des Rosiers, C., Gerszten, R., Glatz, J.F., Griffin, J.L., et al.; American Heart Association Council on Basic Cardiovascular Sciences (2016). Assessing Cardiac Metabolism: A Scientific Statement From the American Heart Association. Circ. Res. *118*, 1659–1701.

Ushikubo, S., Aoyama, T., Kamijo, T., Wanders, R.J., Rinaldo, P., Vockley, J., and Hashimoto, T. (1996). Molecular characterization of mitochondrial trifunctional protein deficiency: formation of the enzyme complex is important for stabilization of both alpha- and beta-subunits. Am. J. Hum. Genet. *58*, 979–988.

**Cell Reports, Volume *23***

## Supplemental Information

# MOXI Is a Mitochondrial Micropeptide That Enhances Fatty Acid β-Oxidation

**Catherine A. Makarewich, Kedryn K. Baskin, Amir Z. Munir, Svetlana Bezprozvannaya, Gaurav Sharma, Chalermchai Khemtong, Akansha M. Shah, John R. McAnally, Craig R. Malloy, Luke I. Szweda, Rhonda Bassel-Duby, and Eric N. Olson**

**SUPPLEMENTAL INFORMATION**

Figures S1-S4.

Tables S1-S3. Related to Figure 2.

Supplemental Experimental Procedures.

Supplemental References.

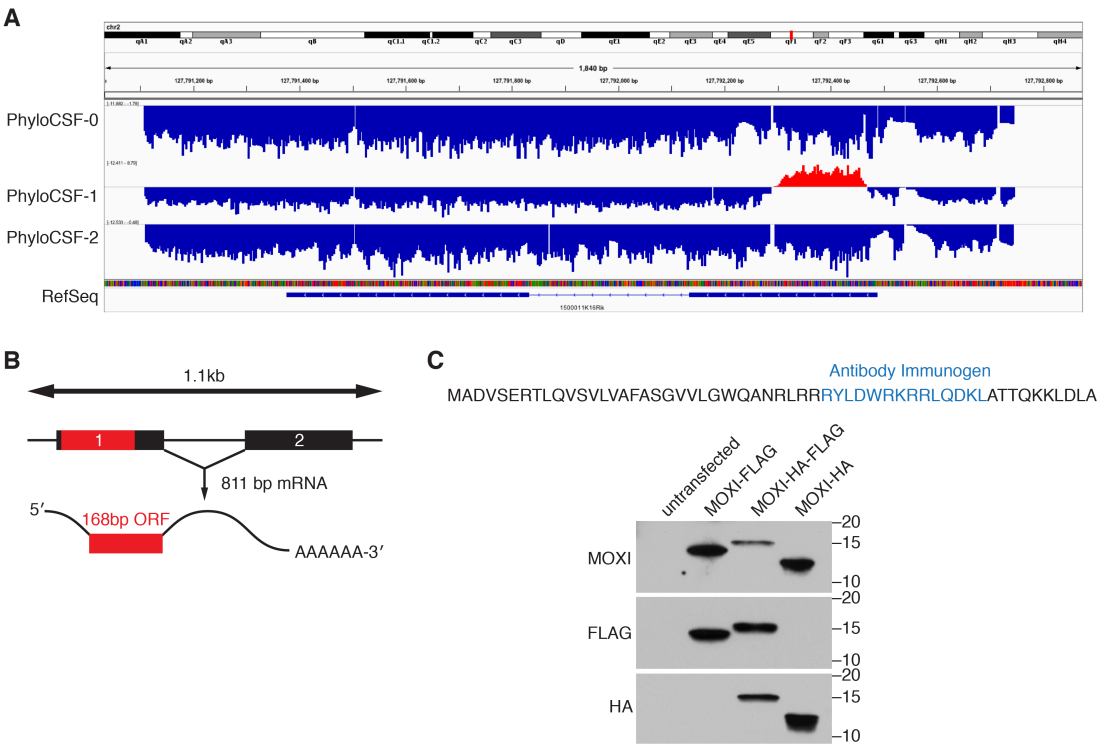


**Figure S1. Overview of the *Moxi* Locus and Antibody Validation. Related to Figure 1.**

(**A**) PhyloCSF score plot for the *Moxi* locus as seen in the UCSC genome browser using the PhyloCSF track hub. The region highlighted in red indicates a positive PhyloCSF score and corresponds with the MOXI ORF.

(**B**) In mice, *Moxi* is transcribed from a 1.1 kilobase (kb) locus on chromosome 2 to produce a transcript of approximately 800 base pairs (bp). The predicted open reading frame (highlighted in red) is contained entirely within the first exon. The transcript is annotated as *1500011K16Rik* and *LINC00116* in the mouse and human genomes, respectively.

(**C**) A custom antibody was raised against the MOXI peptide and validated by Western blot analysis of HEK293 cells transfected with the indicated fusion proteins. Further validation was performed in skeletal muscle and heart tissues from wild-type and MOXI KO mice (Figures 3A and 3B).

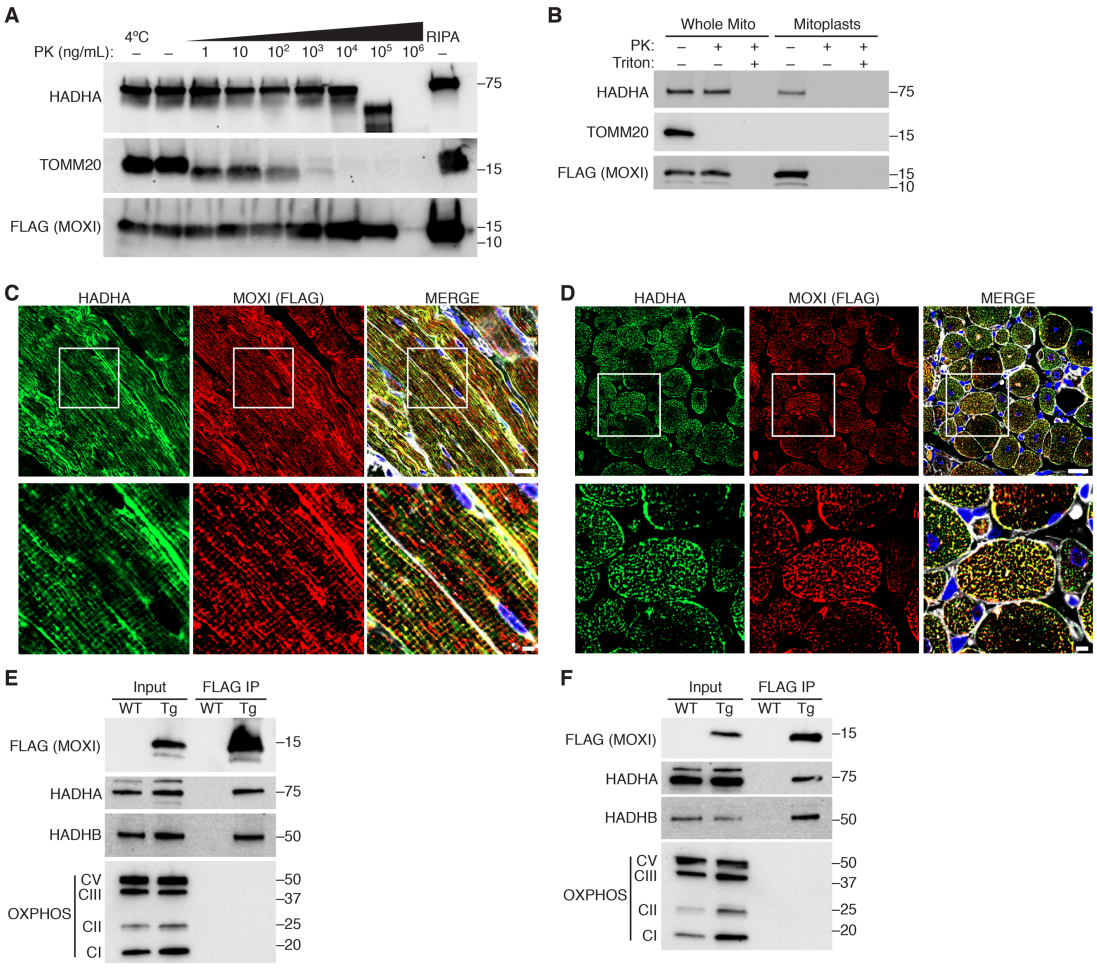


**Figure S2. Validation of Proper IMM Localization of MOXI-FLAG in MCK Transgenic Mice and its Interaction with the MTP. Related to Figure 2.**

(**A**) Mitochondria were isolated from quadriceps muscle from adult MCK-MOXI-FLAG transgenic mice and subjected to proteinase K (PK) digestion at the indicated concentrations at 37°C unless otherwise indicated. Far right, mitochondria lysed in RIPA buffer serves as a control for the total mitochondrial fraction. Western blots were performed for markers of the OMM (TOMM20), IMM (HADHA) or MOXI-FLAG (FLAG).

(**B**) Adult mouse quadriceps mitochondria from MCK-MOXI-FLAG transgenic mice were subjected to PK proteolysis to digest exposed proteins in the presence or absence of detergent (Triton). Osmotic shock was used to isolate mitoplasts which were also subjected to PK digestion. Western blot analysis was performed using antibodies for MOXI-FLAG (FLAG) or for the sub-mitochondrial markers HADHA and TOMM20.

(**C, D**) Longitudinal (**C**) and transverse (**D**) sections of quadriceps muscle from MCK-MOXI-FLAG TG mice were immunostained with antibodies for HADHA (green) and FLAG (red) and imaged by confocal microscopy. Co-localization of MOXI-FLAG with the IMM protein HADHA is evident by yellow signal in the merged image. The merge image also includes DAPI (blue), which labels the nuclei of the muscle fibers, and wheat germ agglutinin (WGA, white), which marks the membranes of the fibers. Low magnification images are displayed on top (scale bar, 20μm) and high magnification images are below (scale bar, 5μm).

(**E, F**) Western blots analysis of FLAG IPs from gastrocnemius/plantaris (**E**) and heart (**F**) homogenates of WT and MCK-MOXI-FLAG TG mice using antibodies for HADHA, HADHB, FLAG, and an OXPHOS cocktail that detects Complex I, II, III and V of the OXPHOS complex. The interaction of MOXI-FLAG with the MTP in the IMM appears to be specific as subunits of the highly abundant OXPHOS complex are excluded from the bound fractions.

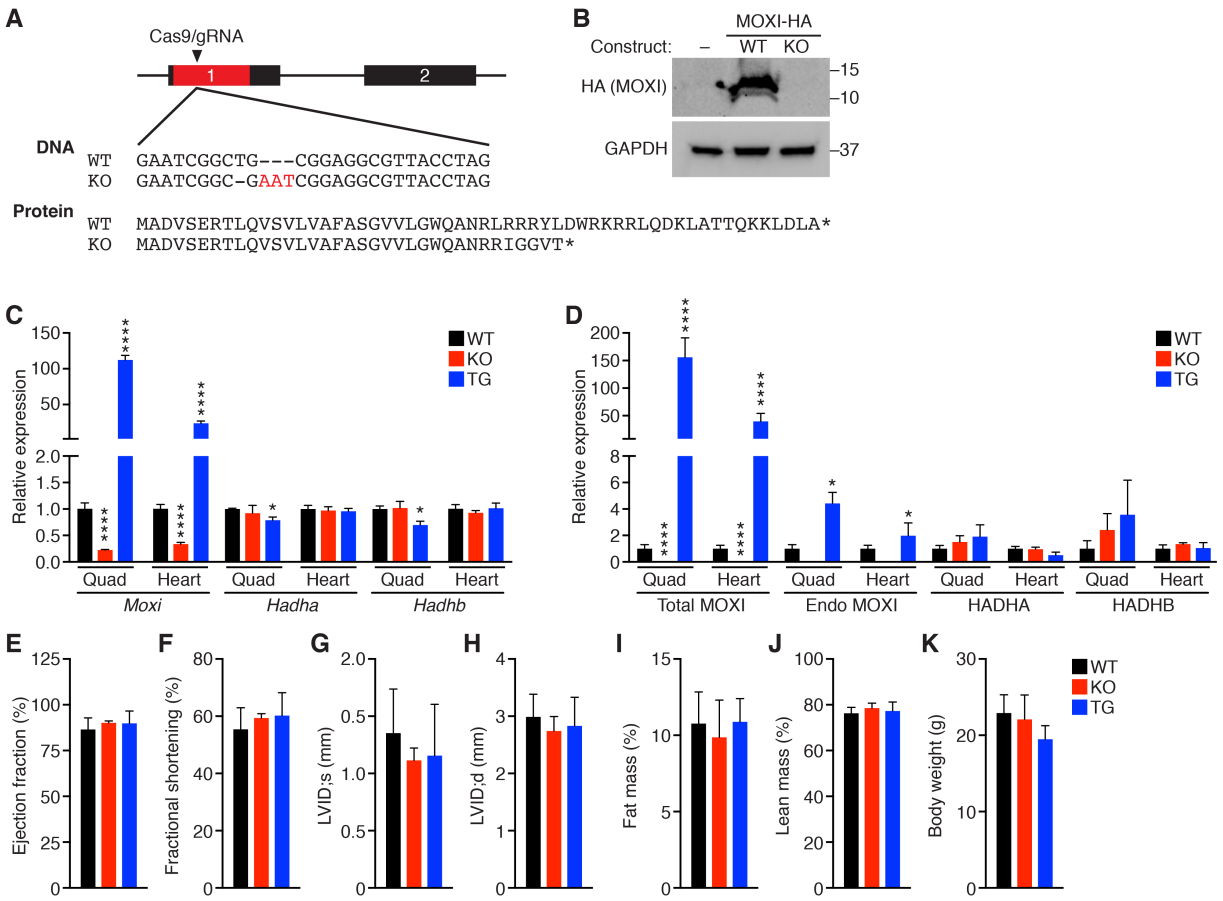


**Figure S3. Generation and Baseline Phenotyping of MOXI knockout and transgenic mice. Related to Figure 3.**

(**A**) A CRISPR gRNA was generated to target the coding sequence of MOXI. An allele containing a 1-bp deletion and 3-bp insertion that creates a frame-shift and premature stop codon was chosen for further experiments.

(**B**) The mutant MOXI sequence created by the CRISPR strategy was cloned and analyzed for stability by Western blot. When transfected in HEK293 cells, the wild-type MOXI-HA fusion protein produces a stable protein while the knockout clone cannot be detected.

(**C**) RNA expression levels of the indicated genes were analyzed in quadriceps and heart tissue of WT, KO and TG mice by qRT-PCR. Data are expressed as mean ± SD for n = 4 mice with significance indicated as *p < 0.05, ****p < 0.001.

(**D**) Quantification of protein expression levels by Western blot analysis of quadriceps and heart tissue of WT, KO and TG mice. Data are expressed as mean ± SD for n = 8 mice with significance indicated as *p < 0.05, ****p < 0.001. Total MOXI expression (FLAG-tagged and untagged MOXI) and the endogenous (Endo) MOXI protein were quantified separately.

(**E-H**) Echocardiography was performed on adult male mice and cardiac function (**E**, **F**) and dimensions (**G**, **H**) were calculated from M-mode images. Data are expressed as mean ± SD for n = 12 WT and KO mice and n = 7 TG mice. LVID, left ventricular internal diameter; s, systole; d, diastole.

(**I-K**) Body composition was measured in adult male mice. Fat mass (**I**) and lean mass (**J**) were analyzed by live magnetic resonance imaging (MRI) and were expressed as a percentage of total body weight (**K**) for n = 10 mice.

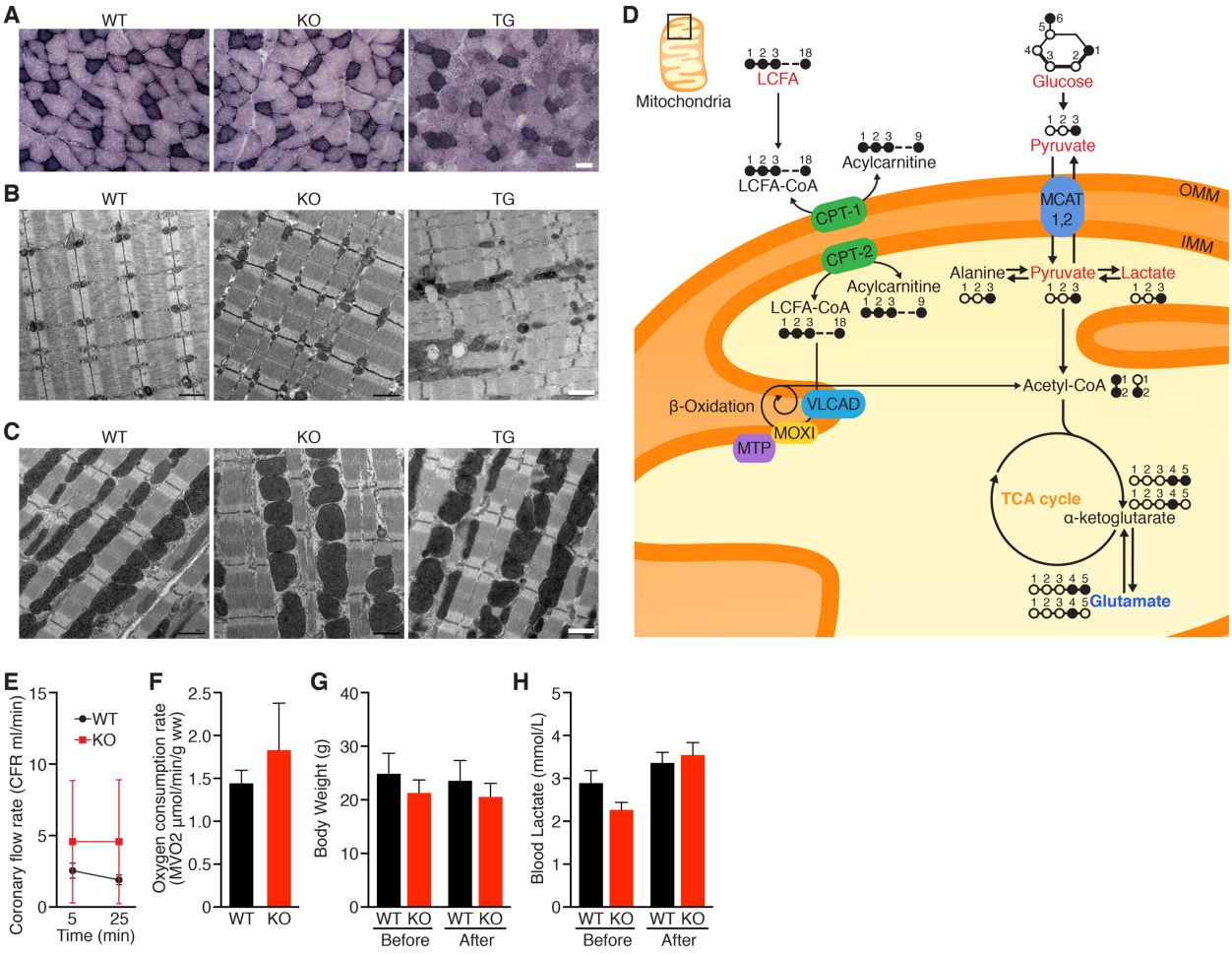


**Figure S4. Mitochondrial Abnormalities in KO and TG Mice. Related to Figures 3 and 4.**

(**A**) Brightfield images of transverse cryosections of quadriceps muscle from WT, KO and TG mice after succinate dehydrogenase (SDH) staining. Representative images from n = 4 mice are shown. Scale bar, 100µm.

(**B, C**) Transmission electron micrographs of quadriceps muscle (**B**) and heart (**C**) from WT, KO and TG mice at low magnification. Scale bar, 1µm. Representative images from n = 3 mice are shown.

(**D**) Illustration of carbohydrate vs long chain fatty acid substrate selection metabolism used for $^{13}$C-NMR isotopomer and flux analyses (related to Figure 4A-F).

(**E**, **F**) Coronary flow rates (**E**) and oxygen consumption rates (**F**) were assessed during perfusion of WT and KO hearts for $^{13}$C-NMR isotopomer studies. Data are presented as mean ± SEM for n = 4 mice per genotype.

(**G, H**) Body weight (**G**) and blood lactate levels (**H**) measured in WT and KO mice before and after forced treadmill running (related to Figure 4G and 4H). Data are represented as mean ± SD for n = 14 mice.

**Table S1**. Unique peptides identified by mass spectrometry of the trifunctional enzyme subunit alpha (HADHA). Percent Coverage: 40.6%. Related to Figure 2.

| Position | Probability | Charge / Sequence | Number of instances |
|---|---|---|---|
| 39 - 46 | 0.9858 | THINYGVK | 1 |
| 47 - 53 | 0.9994 | GDVAVIR | 3 |
| 54 - 60 | 0.9855 | INSPNSK | 1 |
| 119 - 125 | 0.9984 | ISQEGQR | 3 |
| 126 - 132 | 0.1546 | MFEKLEK | 3 |
| 191 - 205 | 0.9996 | MVGVPAAFDMMLTGR | 35 |
| 215 - 230 | 0.9996 | MGLVDQLVEPLGPGIK | 9 |
| 215 - 235 | 0.9996 | MGLVDQLVEPLGPGIKSPEER | 3 |
| 268 - 279 | 0.9996 | LTTYAMTVPFVR | 15 |
| 280 - 289 | 0.0589 | QQVYKTVEEK | 1 |
| 285 - 292 | 0.1252 | TVEEKVKK | 1 |
| 310 - 326 | 0.9996 | AGLEQGSDAGYLAESQK | 8 |
| 327 - 334 | 0.9996 | FGELALTK | 11 |
| 327 - 337 | 0.9996 | FGELALTKESK | 2 |
| 338 - 350 | 0.9977 | ALMGLYNGQVLCK | 3 |
| 387 - 399 | 0.9996 | TLLKDTTVTGLGR | 3 |
| 391 - 399 | 0.9996 | DTTVTGLGR | 1 |
| 400 - 406 | 0.9995 | GQQQVFK | 2 |
| 416 - 422 | 0.9972 | ALTSFER | 2 |
| 461 - 489 | 0.9996 | EVESVTPEHCIFASNTSALPINQIAAVSK | 2 |
| 506 - 516 | 0.9994 | MQLLEIITTDK | 6 |
| 517 - 531 | 0.9996 | TSKDTTASAVAVGLR | 2 |
| 520 - 531 | 0.9996 | DTTASAVAVGLR | 5 |
| 520 - 534 | 0.9996 | DTTASAVAVGLRQGK | 3 |
| 532 - 540 | 0.3681 | QGKVIIVVK | 1 |
| 541 - 549 | 0.9996 | DGPGFYTTR | 2 |
| 550 - 560 | 0.9996 | CLAPMMSEVMR | 23 |
| 561 - 569 | 0.9996 | ILQEGVDPK | 14 |
| 632 - 644 | 0.4449 | SGKGFYIYQEGSK | 2 |
| 635 - 644 | 0.9996 | GFYIYQEGSK | 2 |
| 647 - 660 | 0.9995 | SLNSEMDNILANLR | 8 |
| 661 - 676 | 0.9996 | LPAKPEVSSDEDVQYR | 5 |
| 720 - 728 | 0.9996 | FVDLYGAQK | 1 |

**Table S2**. Unique peptides identified by mass spectrometry of the trifunctional enzyme subunit beta (HADHB). Percent Coverage: 37.9%. Related to Figure 2.

| Position | Probability | Sequence | Number of instances |
|---|---|---|---|
| 43 - 53 | 0.311 | SKKTLAKPNMK | 2 |
| 46 - 53 | 0.9519 | TLAKPNMK | 2 |
| 63 - 73 | 0.9996 | IPFLLSGTSYK | 4 |
| 83 - 91 | 0.9996 | AALSGLLHR | 4 |
| 119 - 129 | 0.9996 | EAALGAGFSDK | 2 |
| 183 - 189 | 0.974 | MMLDLNK | 2 |
| 183 - 191 | 0.3303 | MMLDLNKAK | 3 |
| 231 - 239 | 0.9996 | LAAAFAVSR | 7 |
| 240 - 248 | 0.9996 | MEQDEYALR | 22 |
| 256 - 269 | 0.9754 | AQDEGHLSDIVPFK | 2 |
| 279 - 292 | 0.9996 | DNGIRPSSLEQMAK | 9 |
| 327 - 335 | 0.9996 | ALAMGYKPK | 5 |
| 340 - 349 | 0.9996 | DFIYVSQDPK | 2 |
| 340 - 362 | 0.9996 | DFIYVSQDPKDQLLLGPTYATPK | 3 |
| 350 - 362 | 0.9996 | DQLLLGPTYATPK | 18 |
| 393 - 406 | 0.9995 | AMDSDWFAQNYMGR | 8 |
| 408 - 417 | 0.74 | TKVGSPPLEK | 2 |
| 449 - 475 | 0.9813 | DGGQYALVAACAAGGQGHAMIVEAYPK | 2 |

**Table S3**. Unique peptides identified by mass spectrometry of MOXI-FLAG. Percent Coverage: 58.8%. Related to Figure 2.

| Position | Probability | Charge / Sequence | Number of instances |
|---|---|---|---|
| 8 - 29 | 0.9993 | TLQVSVLVAFASGVVLGWQANR | 1 |
| 8 - 31 | 0.9993 | TLQVSVLVAFASGVVLGWQANRLR | 2 |
| 52 - 58 | 0.9961 | KLDLASR | 6 |
| 62 - 80 | 0.9993 | DHDGDYKDHDIDYKDDDDK | 41 |
| 69 - 80 | 0.0554 | DHDIDYKDDDDK | 1 |

## SUPPLEMENTAL EXPERIMENTAL PROCEDURES

**Animals.** All animal work described in this manuscript has been approved and conducted under the oversight of the UT Southwestern Institutional Animal Care and Use Committee. Transgenic and knockout mouse lines were generated on a pure C57BL/6N background. All functional experiments were performed using 12-16 week old male mice.

**Identification of conserved small open reading frames.** RNA transcripts annotated as noncoding were analyzed using PhyloCSF on the UCSC genome browser (Kent et al., 2002; Lin et al., 2011; Raney et al., 2014). PhyloCSF was used to calculate conservation scores for potential open reading frames (ORFs) in the three reading frames on both strands of DNA (Lin et al., 2011). Regions that scored positively by PhyloCSF were further analyzed manually. The MOXI ORF was found contained within the noncoding transcript *1500011K16Rik* in mice and *LINC00116* in humans.

**In vitro transcription and translation.** The full-length *Moxi* and *Pln* RNAs were subcloned into pcDNA3.1(+) (Invitrogen) containing the T7 RNA polymerase promoter. Frameshift (FS) mutations were introduced immediately after the endogenous ATG start codon of each transcript to disrupt the open reading frames of the micropeptides using site directed mutagenesis (QuikChange Lightening Site Directed Mutagenesis kit, Agilent Technologies). Coupled in vitro transcription and translation assays were performed using digested linear plasmids and the TNT T7 Coupled Wheat Germ Extract System (Promega), as per the manufacturer's protocol. Reactions were setup with radiolabeled [$^{35}$S]methionine (PerkinElmer). Products were resolved on 18% SDS–polyacrylamide gels, dried, and exposed to film for 48 hours at room temperature.

**Quantitative mRNA measurement**. Total RNA was extracted from adult mouse tissues using Trizol and reverse transcribed using iScript Reverse Transcription Supermix (Bio-Rad) with random primers. Quantitative Polymerase Chain Reaction (qPCR) samples were assembled using KAPA SYBR Fast qPCR Master Mix (SIGMA). Assays were performed using a 7900HT Fast Real-Time PCR machine (Applied Biosystems). Expression amount was normalized to 18S mRNA and was represented as fold change. The following oligonucleotides were ordered from Integrated DNA Technologies to measure transcript abundance:

**18s Forward: 5′**- ACC GCA GCT AGG AAT AAT GGA -**3′**

**18s Reverse: 5′**- GCC TCA GTT CCG AAA ACC A -**3′**

**MOXI Forward: 5′**- GTG TCC GTG CTA GTG GCT TT -**3′**

**MOXI Reverse: 5′**- CCA GGT CCA GCT TTT TCT GA -**3′**

**Hadha Forward: 5′**- TGC ATT TGC CGC AGC TTT AC -**3′**

**Hadha Reverse: 5′**- GTT GGC CCA GAT TTC GTT CA -**3′**

**Hadhb Forward: 5′**- ACT ACA TCA AAA TGG GCT CTC AG -**3′**

**Hadhb Reverse: 5′**- AGC AGA AAT GGA ATG CGG ACC -**3′**

**Tissue western blot analysis.** Tissues were collected and snap frozen in liquid nitrogen. Frozen samples were pulverized and then homogenized in RIPA buffer (SIGMA) with added cOmplete, EDTA-free protease inhibitor cocktail (Roche) and PhosSTOP phosphatase inhibitors (Roche) on ice using a glass WHEATON Dounce tissue grinder ('tight'). Protein concentration was determined using a Pierce BCA Protein Assay Kit (ThermoFisher Scientific). Samples were separated on Mini-PROTEAN TGX Precast Gels (Bio-Rad) or bis/acrylamide gels made by standard gel preparation. Gels were transferred to PVDF membrane (Millipore, Immobilon-P), blocked in 5% milk/TBST and then incubated in primary antibodies: MOXI (New England Peptide), 1:500; HADHA (Abcam) 1:1,000; HADHB (BETHYL Laboratories), 1:500; and GAPDH (Millipore), 1:10,000. Western blots were washed in TBST, incubated with fluorescent or HRP-conjugated secondary antibodies (Bio-Rad), and then developed using a ChemiDoc MP Imaging System (Bio-Rad) or autoradiograph film.

**Cell culture, transfections and immunostaining**. C2C12 myoblasts and HEK293 cells (ATCC) were grown and maintained in DMEM containing 10% FBS and penicillin-streptomycin. C2C12 cells were transfected with Lipofectamine 2000 (Invitrogen) and HEK293 cells were transfected with FuGENE 6 Transfection Reagent (Promega) according to the manufacturer's protocol. For immunostaining, C2C12 cells were plated on MatTek glass bottom dishes and transfected for 24 hours. Cells were washed with PBS and then fixed with 4% paraformaldehyde. Fixed cells were permeabilized with 0.1% Triton-X100, blocked with 1% BSA/PBS, and then incubated in primary antibody (rabbit FLAG or mouse FLAG M2, SIGMA) diluted in blocking buffer at 4$^{o}$C overnight. The following day,

cells were washed and incubated with Alexa Fluor (Invitrogen) fluorescent secondary antibodies and DAPI (SIGMA). Samples were imaged using a Zeiss LSM-800 confocal with a 40X oil objective.

**Mitochondrial subfractionation and proteinase K digestion assays.** Quadriceps muscles were isolated from mice and homogenized with a Teflon Potter dounce in isolation buffer (75 mM sucrose, 225 mM mannitol, 5 mM HEPES and 1 mM EGTA, pH 7.4). Homogenates were centrifuged at 2,000xg and then the supernatants were transferred to fresh tubes and re-centrifuged at 14,000xg. The pellets were resuspended in isolation buffer and spun again at 14,000xg. The pellet was resuspended in assay buffer (125 mM KCl, 20 mM HEPES, 2 mM $MgCl_2$, 2 mM $KH_2PO_4$ and 0.04 mM EGTA, pH 7.2). For proteinase K gradient experiments, mitochondrial samples were incubated with a range of PK concentrations from 1 ng/mL to 1 mg/mL at 37°C and then analyzed by gel electrophoresis and Western blotting. For subfractionation experiments, mitochondria were swollen in hypotonic 10 mM $KH_2PO_4$ buffer (pH 7.4) and then one-third the volume of hypertonic buffer (1.8 M sucrose, 10 mM $MgCl_2$, pH 7.4) was added to shrink the mitochondria. Samples were sonicated and then centrifuged at 12,000xg. The pellet was resuspended in hypertonic buffer and centrifuged at 12,000xg. The pellet derived from this spin was the mitoplast fraction. This was then either kept as the total mitoplast fraction or re-swollen in hypotonic buffer and shrunk in hypertonic buffer to disrupt the inner mitochondrial membrane. Where indicated, samples were treated with Triton X-100 at a final concentration of 1%.

**Generation of mouse lines.** Animal work described in this manuscript has been approved and conducted under the oversight of the UT Southwestern Institutional Animal Care and Use Committee. All mouse lines were generated on a pure C57BL/6N background. Muscle creatine kinase (MCK) transgenic (TG) mice were made as previously described by placing the murine MOXI cDNA fused with a C-terminal FLAG tag under the control of a 4.8-kb fragment of the MCK promoter (Sternberg et al., 1988) and deriving transgenic mice on a C57BL/6N background. All analyses were done within the same line using wild-type littermates as controls. For genotyping, tail biopsies were collected and treated with an alkaline lysis buffer (25 mM NaOH, 0.2 mM EDTA) at 95°C, followed by neutralization with 40 mM Tris-HCl. Transgenic mice were genotyped based on the presence or absence of the hGH sequence and myogenin primers were used as a positive control. The following primers were used for genotyping:

**hGH Forward: 5'**- GTC TGA CTA GGT GTC CTT CT -**3'**

**hGH Reverse: 5'**- CGT CCT CCT GCT GGT ATA G -**3'**

**Myogenin Forward: 5'**- TTA CGT CCA TCG TGG ACA GC -**3'**

**Myogenin Reverse: 5'**- TGG GCT GGG TGT TAG CCT TA -**3'**

KO mice were generated using the clustered regularly interspaced short palindromic repeats (CRISPR)-associated protein 9 (Cas9) gene-editing system by pronuclear and cytoplasmic injection of mouse embryos with Moxi guide RNA (gRNA) and Cas9 mRNA as previously described (Long et al., 2014). Briefly, a gRNA targeting the first exon of *Moxi* was designed using http://crispr.mit.edu/ and cloned into Addgene plasmid #42230 (Cong et al., 2013), a gift from Feng Zhang, using the following primers:

**Moxi guide Forward: 5′-** CAC CGG GCA AGC GAA TCG GCT GCG G **-3′**

**Moxi guide Reverse: 5′-** AAA CCC GCA GCC GAT TCG CTT GCC **-3′**

Cleavage efficiency was tested in cell culture using 10T1/2 mouse fibroblasts. The gRNA was transcribed in vitro and spin-column purified, while the Cas9 mRNA was obtained commercially (TriLink Biotechnologies). Mouse embryos were injected with an equal ratio (w/w) of gRNA and Cas9 mRNA into the pronucleus and cytoplasm and transferred to a surrogate dam for gestation. Mosaic C57BL/6N $F_0$ founders were identified by T7E1 assay on tail biopsies, and positive founders were bred to wild-type C57BL/6N mice to isolate knockout alleles. Mutants in the F1 generation were identified by T7E1 assay, and the alleles were TOPO TA cloned (Thermo Fisher Scientific) and sequenced. A founder with a 1-base pair deletion and 3-base pair insertion that disrupts the MOXI ORF was chosen for further analysis. Tail DNA was isolated as described above and mice were genotyped using the following primers:

**MOXI KO genotyping Forward: 5′**- AAC GCG GAG CCC ATC AGA AA -**3′**

**MOXI KO genotyping Reverse: 5′**- CCC TCA GCA AAC TGA GCT GT -**3′**

PCR products were run on a 1.5% agarose gel, gel purified, and submitted for sequencing using the MOXI KO genotyping Forward primer.

The guide RNA that we selected to use to generate our MOXI KO mice did not have any predicted off-targets with fewer than 3 base pair mismatches. For thoroughness, we verified that there were no off-target editing events in our KO mice by sequencing the top 25 predicted genome-wide off-target sites. Notably, of these top 25 sites, only 6 are located in exons of coding genes and all of these have greater than 4 base pair mismatches to the guide indicating unlikely targeting. The primer sequences used to amplify and sequence these regions are as follows:

| **Locus** | **Gene** | **Forward** | **Reverse** |
|---|---|---|---|
| chr7:-81596050 | | GAGGAGTCTGGTTTGGGTGA | CCCACAAACTCGGCATAGAT |
| chrX:-34348198 | | AAAAGGGAAGCAGAGGAAGC | CTGTGCTCTGACGTGGGTTA |
| chr7:-125280421 | Smg1 | ATCAACATCTCGGCCCTCTA | CATGAACCACCACTGTGGAA |
| chr6:-39424255 | | CACAGTTGGGTGACAGTTGG | CAAATGCCTCTTCTGCAACA |
| chr14:+56111847 | Lrrc16b | TCTCTCTGGAGAGCGGAGTC | GGATGCTCAGCTCCTGGTAA |
| chr6:+87119752 | | CCAGCCACAGAAGCAATTTT | AACAACCTCCTGGCACAAAC |
| chr7:+145057591 | | CCCAGCTGTGTGACAGAGAA | TAAGGGTAGCAGGAGGCAGA |
| chr6:+7529542 | | ATTGTGGGAATGCAAGAAGG | CGTGGTGAAATGCTGTTTTG |
| chr5:-93026160 | | AAGTGGAAACGCAGCAGATT | ACCGGACATAGGCTGTTTTG |
| chr4:+128369270 | | GGAGCTGGTGTTATGGTGGT | TGCCAGCTGTCTTTCAGATG |
| chr9:+58244183 | | CGGTCGCTGAGATAAGGAAA | GGCATGAGGTGATTTGAGGT |
| chr12:-86217015 | Ltbp2 | TTCTCCGAGTCTGGACAGGT | CGCCATACAGCCCTTACCTA |
| chr1:+190967046 | | CCCCAGACAGCTAGCTCAAG | GGACTGCGTTATCCACAGGT |
| chr3:-127540076 | Ap1ar | GTTCTGTCAAGGCCCAAAAG | GATGGGGAACTGCTGCTG |
| chr1:-120927914 | Gli2 | GGAAGGGGAAGAGGAGTGAG | CACCAAGCTCCACCATCTCT |
| chr14:+122020530 | Dock9 | CTCACTGTGCAACAGCACCT | CGGTTGTCATGTCTTGGATG |
| chr2:+164721570 | Zfp335 | TTTGTAAAAGCGGGAACCTG | GGCTCTGGTAGGATGGTGAA |
| chr11:-104624333 | | CCTTCCTCCAGCTTCTCTCC | TAAAGAGCAAGCACCCTCCA |
| chr18:-28221255 | | AAGCCTGAAAGGGTCAAACA | AGTAAATACCGAGGCCAAAGC |
| chr2:-166962614 | | TGCACACACAATCACAGGAA | TGGATCTCATTCACGACTGC |
| chr10:-74305478 | | CCAGTTGCTCTGCCAAATAA | GTTTGGGAGGTTTGGTCTGA |
| chr10:+31055340 | Tpd52l1 | ACCTTGAAGCACATGCCTTT | GCCCAACCCTACAGTTCAAA |
| chr7:+59316103 | | TTGCCCTGGGAAAATAATTAAA | CATTTCCTAAGCCCGGTATG |
| chr3:-55458365 | | TGATATGGTGGTAGGCAGCA | AAGTCACCTGTGGCCATCTT |
| chr12:+45076178 | | CTCCCTGAAACCTGCAAAAG | TGTTTGGAGGAATGGTCACA |

There were no off-target CRISPR editing events identified in any of the regions analyzed.

**Tissue immunoprecipitations (IPs) and proteomics.** For the identification of MOXI-interacting proteins, quadriceps muscles were isolated from MCK-MOXI-FLAG TG mice and wild-type littermate controls. Tissues were homogenized with a Teflon Potter dounce in IP Buffer (25 mM Tris, 150 mM NaCl, 1 mM EDTA, 1% NP-40 and 5% glycerol, pH 7.4) containing cOmplete, EDTA-free protease inhibitor cocktail (Roche) and PhosSTOP phosphatase inhibitors (Roche). Homogenates were spun at 2,000xg at 4$^{o}$C and supernatants were transferred to a clean tube. Samples were lightly sonicated on ice and then incubated with Anti-FLAG M2 magnetic beads (SIGMA) that were pre-blocked with 1% BSA. Samples were rotated overnight at 4$^{o}$C and then washed 10 times with IP Wash Buffer (25 mM Tris, 700 mM NaCl, 1 mM EDTA, 1% NP-40 and 5% glycerol, pH 7.4). Bound proteins were eluted using 3XFLAG peptide (SIGMA) in IP Buffer at 4$^{o}$C as per manufacturer's instructions. Tissue homogenates, FLAG eluted

proteins and the unbound protein fractions were run on a 4-20% Mini-PROTEAN TGX gel (Bio-Rad) and silver stained using a SilverQuest Silver Staining Kit (Invitrogen). Silver stained bands that were unique to the TG sample were cut out and submitted to the University of Texas Southwestern Medical Center Proteomics Core facility for protein identification using LC-MS/MS as previously described (Garg et al., 2014). Proteins that were identified by Mass Spec were validated by Western blotting using the following antibodies: FLAG M2-Peroxidase (HRP), 1:1,000 (SIGMA); HADHA, 1:1,000 (Abcam); HADHB, 1:500 (BETHYL Laboratories); Total OXPHOS rodent WB antibody cocktail, 1:1,000 (Abcam). Tissue IPs were repeated using gastrocnemius/plantaris muscles and hearts from WT and TG mice and results were validated by Western blot.

For the identification of endogenous MOXI protein by mass spec analysis, quadriceps muscles were isolated from adult wild-type mice and homogenates were made as described above. Samples were immunoprecipitated with MOXI primary antibody (New England Peptide) and the bound proteins were captured using magnetic Dynabeads (Invitrogen) and eluted by boiling in Laemmli Buffer (Bio-Rad). Eluted proteins were run on a 4-20% Mini-PROTEAN TGX gel (Bio-Rad) and coomassie stained using EZBlue Gel Staining Reagent (SIGMA). The region of the gel corresponding to the molecular weight of MOXI (below 10kDa) was isolated and submitted to the University of Texas Southwestern Medical Center Proteomics Core facility for protein identification using elastase in-gel digestion and LC-MS/MS analysis as previously described (Garg et al., 2014).

**Immunoprecipitations in transfected cells**. Co-IPs were performed as previously described (Anderson et al., 2015; Nelson et al., 2016). Briefly, HEK293 cells were transfected with expression plasmids encoding Myc-HADHA, HADHB-FLAG or empty FLAG vector control, and MOXI-HA or HA-DWORF using FuGENE 6 Transfection Reagent (Promega). Cells were washed with PBS and then scraped and collected in IP Buffer (25 mM Tris, 150 mM NaCl, 1 mM EDTA, 1% NP-40 and 5% glycerol, pH 7.4) containing cOmplete, EDTA-free protease inhibitor cocktail (Roche) and PhosSTOP phosphatase inhibitors (Roche). The same protocol detailed above for tissue IPs was followed for lysate preparation, FLAG IP and FLAG elution in transfected cells. Western blots were performed using the following antibodies: FLAG M2-Peroxidase (HRP), 1:1,000 (SIGMA); HADHA, 1:1,000 (Abcam); Myc, 1:1,000 (Invitrogen); HA clone (5B1D10), 1:1,000 (Invitrogen) and GAPDH (Millipore), 1:10,000.

**Transthoracic echocardiography**. Cardiac function and heart dimensions were determined in 12-16 week old male mice by two-dimensional echocardiography using a Visual Sonics Vevo 2100 Ultrasound (Visual Sonics, Canada) on unanesthetized mice. Motion (M)-mode tracings were used to measure anterior and posterior wall thicknesses at end diastole and end systole. Left ventricular (LV) internal diameter (LVID) was measured as the largest anteroposterior diameter in either diastole (LVIDd) or systole (LVIDs). A single observer blinded to mouse genotypes performed echocardiography and data analysis. Fractional shortening (FS) was calculated according to the following formula: FS(%) = [(LVIDd-LVIDs)/LVIDd] X 100. Ejection fraction (EF%) was calculated by: EF(%) = EDV-ESV/EDV (ESV, end systolic volume; EDV, end diastolic volume).

**Body composition measurements.** Live 12-16 week old male mice were analyzed for total body fat, lean tissue and body water content using an EchoMRI quantitative magnetic resonance system (Echo Medical Systems).

**Histology and immunofluorescence.** For enzyme histochemistry, skeletal muscle tissues were isolated and embedded in a mixture of OCT (Fisher) and gum tragacanth (Sigma-Aldrich) and flash-frozen in a 2-methybutane reservoir submerged in liquid nitrogen, followed by cryostat sectioning at 10 μM. Sections were submitted to the University of Texas Southwestern Medical Center Molecular Pathology Core for enzyme histochemistry (succinate dehyrdeogenase, SDH). For immunofluorescent staining, frozen sections were air-dried, fixed with 1% PFA and permeabilized with PBST (0.3% Tween-20/PBS). Sections were blocked with 5% donkey serum (Sigma-Aldrich) in PBST and then incubated in primary antibody in blocking buffer at 4˚C in a humidified chamber using the following antibodies: HADHA (Abcam), FLAG M2 (SIGMA), Desmin (Dako), Laminin (SIGMA). The following day, samples were washed and incubated with the appropriate Alexa Fluor (Invitrogen) fluorescent secondary antibodies, Wheat Germ Agglutinin (Invitrogen) and DAPI (SIGMA). Samples were washed again and coverslips were mounted using VECTASHIELD Antifade Mounting Media (VECTOR Laboratories). Confocal images were taken with a Zeiss LSM-800 using a 40X oil objective. For routine histology, samples were isolated and fixed in 4% (vol/vol) paraformaldehyde in PBS for 48 hours at room temperature with gentle shaking. Samples were dehydrated, embedded in paraffin, sectioned and stained with hematoxylin and eosin (H&E) using standard procedures.

**Transmission electron microscopy**. 12-week old male mice were perfusion fixed by transcardial perfusion using 4% paraformaldehyde and 1% glutaraldehyde in 0.1 M sodium cacodylate buffer (pH 7.4). Tissues were collected and samples were processed by the University of Texas Southwestern Medical Center Electron Microscopy Core facility.

Briefly, fixed tissues were post-fixed, stained, dehydrated, and embedded in EMbed-812 resin. Tissue sections were cut and post-stained, and images were acquired on a FEI Tecnai G2 Spirit TEM.

**DNA extraction from tissue for mtDNA quantification.** Tissues from 12-16 week old male mice were homogenized in Trizol and then separated using chloroform. The aqueous phase containing RNA was removed and back extraction buffer (4 M guanidine thiocyanate, 50 mM sodium citrate, 1M Tris) was added to the remaining interphase and organic phase. Samples were mixed, incubated at room temperature, and then centrifuged at 3,000xg at 4°C. The upper phase containing the DNA was transferred to a new tube and precipitated with isopropanol with polyacryl carrier. Samples were mixed and then centrifuged at 12,000xg at 4°C. Pellets were washed with 75% ethanol four times and then air dried and resuspended in 8 mM NaOH. After DNA was resuspended, 1 M Hepes was added to a final concentration of 10 mM and 100 mM EDTA was added to a final concentration of 1 mM. qPCR was performed using KAPA SYBR Fast qPCR Master Mix (SIGMA) as described above. The following primer sets were used for qPCR:

**NADH dehydrogenase subunit 1 (MT-ND1) Forward**: **5′-** CCC ATT CGC GTT ATT CTT **-3′**

**NADH dehydrogenase subunit 1 Reverse: 5′-** AAG TTG ATC GTA ACG GAA GC **-3′**

**Lipoprotein Lipase (LPL) Forward**: **5′-** GGA TGG ACG GTA AGA GTG ATT C **-3′**

**Lipoprotein Lipase Reverse: 5′-** ATC CAA GGG TAG CAG ACA GGT **-3′**

**Treadmill exercise**. 12-16 week old male mice were run on Exer-3/6 treadmill apparatus (Columbus Instruments) with mild electrical stimulus. Two days before the experiment, mice were acclimatized to a single lane treadmill by performing a 10 m/min run for 10 min. For the experimental test, the treadmill was set to ramp from 0 to 10 m/min over a period of 5 minutes and then stay at 10 m/min for an additional 5 minutes. The treadmill speed then incrementally increased (1m/min every 5 min) to a maximum speed of 20 m/min until exhaustion. Exhaustion was defined by failure to run for greater than 10 sec.

**Mitochondrial isolations for functional analysis.** Quadriceps muscle and hearts were isolated from 12-16 week old male mice and homogenized in ice cold isolation buffer (10 mM MOPS, 210 mM mannitol, 70 mM sucrose and 1mM EDTA, pH 7.4) with a Teflon Potter dounce. Homogenates were centrifuged at 800xg and the supernatants were collected and centrifuged again at 8,000xg. The pellet was resuspended in isolation buffer and then centrifuged a final time at 8,000xg. The pellet was resuspended in STE buffer (250 mM sucrose, 10 mM Tris-HCl, 1 mM EDTA, pH 7.4) for fatty acid oxidation rate assays or isolation buffer for mitochondrial respiratory function analysis.

**Long chain fatty acid oxidation assays**. Oxidation of [1-$^{14}$C]palmitic acid by mitochondria isolated from quadriceps muscle or hearts of WT and MOXI KO mice was analyzed using a detailed published protocol (Huynh et al., 2014). Briefly, mitochondria were isolated as described above and resuspended in STE buffer (250 mM sucrose, 10 mM Tris-HCl, 1 mM EDTA, pH 7.4). Mitochondria were incubated in oxidation reaction buffer (100 mM sucrose, 10 mM Tris-HCl, 5 mM $KH_2PO_4$, 0.2 mM EDTA, 80 mM KCl, 1 mM $MgCl_2$, 2 mM L-carnitine, 0.1 mM malate, 0.05 mM coenzyme A, 2 mM ATP, 1 mM DTT and 0.7% BSA/0.1 mM palmitate/0.4 μCi $^{14}$C-palmitate) for one hour and then transferred to tubes containing 1 M perchloric acid. Fully oxidized $CO_2$ was captured on Whatman filter paper discs treated with 1 M NaOH placed in the lids of the tubes. After incubation for one hour with gentle agitation, the Whatman filter paper discs were transferred to scintillation vials for counting and the reaction mixture was then centrifuged at 14,000xg. The supernatant containing the acid-soluble metabolites (ASMs) was transferred to a scintillation vial for counting and analysis. Where indicated, samples were pre-incubated with 40 μM etomoxir for 5 minutes on ice before addition of the oxidation reaction buffer.

**Analysis of mitochondrial respiratory function.** Isolated mitochondria were diluted to 0.25 mg/mL (heart) or 0.5 mg/mL (quadriceps) in respiratory buffer composed of 10 mM MOPS, 210 mM mannitol, 70 mM sucrose and 5 mM $K_2HPO_4$ at pH 7.4 containing the following respiratory substrates: 1 mM malate and palmitoylcarnitine (25 μM for heart, 50 μM for quad) or 100 μM pyruvate. For measurements with quadriceps mitochondria, 1.25 mM $MgCl_2$ was also included in the respiratory buffer. State 3 respiration was initiated after 2 minutes with the addition of ADP at a final concentration of 0.25 mM. Rates of mitochondrial respiration were evaluated at room temperature using a Neofox oxygen chamber with a 175 μL volume (Instech Laboratories) (Crewe et al., 2013).

**$^{13}$C-NMR isotopomer analysis.** Hearts were quickly excised after cervical dislocation of mice. Hearts were cannulated via aorta, connected to a perfusion column apparatus and maintained at 37 °C with a controlled temperature bath. Hearts were perfused for 30 min at 100 cm $H_2O$ pressure with a modified Krebs-Henseleit (KH) buffer containing 8 mM [1,6-$^{13}$C]glucose, 1.2 mM [3-$^{13}$C]lactate, 0.12 mM [3-$^{13}$C]pyruvate, 0.4 mM [U-$^{13}$C]long chain fatty acids

(LCFA), 0.75% bovine serum albumin (BSA) and 2.5 mM $CaCl_2$ equilibrated with 95:5 $O_2$:$CO_2$. Cardiac function was monitored during the perfusion with a fluid-filled catheter in the left ventricle. Coronary flow samples were collected at 5 and 25 minutes to measure oxygen consumption using a blood gas analyzer (Instrumentation Laboratory, Lexington, MA). After 30 min of perfusion, hearts were snap-frozen in liquid nitrogen. The frozen tissues were pulverized in liquid nitrogen and extracted with perchloric acid (4%), neutralized, and reconstituted in $D_2O$ containing 1 mM EDTA and 0.5 mM 2,2-dimethyl-2-silapentane-5-sulfonate (DSS) standard. Proton-decoupled $^{13}$C-NMR spectra of heart extracts were acquired at 600 MHz spectrometer (Bruker Corporation, USA) equipped with 5-mm cryoprobe. $^{13}$C-NMR multiplets from glutamate were deconvoluted using ACD/SpecManager (ACD Labs, Canada) and multiplet ratios to determine the relative oxidation of [1,6-$^{13}C_2$]glucose, [U-$^{13}$C]LCFA, and unlabeled endogenous substrates (e.g., triglycerides and glycogen). Multiplet ratios were submitted as input in tcaCALC v.2.07 for isotopomer analysis (Baskin et al., 2014). Data presented as the mean ± SEM (n = 4 per group) and analyzed with Welch's t-test for statistical significance.

**SUPPLEMENTAL REFERENCES**


Baskin, K.K., Grueter, C.E., Kusminski, C.M., Holland, W.L., Bookout, A.L., Satapati, S., Kong, Y.M., Burgess, S.C., Malloy, C.R., Scherer, P.E., *et al*. (2014). MED13-dependent signaling from the heart confers leanness by enhancing metabolism in adipose tissue and liver. EMBO Mol Med *6*, 1610-1621.

Cong, L., Ran, F.A., Cox, D., Lin, S., Barretto, R., Habib, N., Hsu, P.D., Wu, X., Jiang, W., Marraffini, L.A., *et al*. (2013). Multiplex genome engineering using CRISPR/Cas systems. Science *339*, 819-823.

Crewe, C., Kinter, M., and Szweda, L.I. (2013). Rapid inhibition of pyruvate dehydrogenase: an initiating event in high dietary fat-induced loss of metabolic flexibility in the heart. PLoS One *8*, e77280.

Garg, A., O'Rourke, J., Long, C., Doering, J., Ravenscroft, G., Bezprozvannaya, S., Nelson, B.R., Beetz, N., Li, L., Chen, S., *et al*. (2014). KLHL40 deficiency destabilizes thin filament proteins and promotes nemaline myopathy. J Clin Invest *124*, 3529-3539.

Huynh, F.K., Green, M.F., Koves, T.R., and Hirschey, M.D. (2014). Measurement of fatty acid oxidation rates in animal tissues and cell lines. Methods Enzymol *542*, 391-405.

Kent, W.J., Sugnet, C.W., Furey, T.S., Roskin, K.M., Pringle, T.H., Zahler, A.M., and Haussler, D. (2002). The human genome browser at UCSC. Genome Res *12*, 996-1006.

Long, C., McAnally, J.R., Shelton, J.M., Mireault, A.A., Bassel-Duby, R., and Olson, E.N. (2014). Prevention of muscular dystrophy in mice by CRISPR/Cas9-mediated editing of germline DNA. Science *345*, 1184-1188.

Raney, B.J., Dreszer, T.R., Barber, G.P., Clawson, H., Fujita, P.A., Wang, T., Nguyen, N., Paten, B., Zweig, A.S., Karolchik, D., *et al*. (2014). Track data hubs enable visualization of user-defined genome-wide annotations on the UCSC Genome Browser. Bioinformatics *30*, 1003-1005.

Sternberg, E.A., Spizz, G., Perry, W.M., Vizard, D., Weil, T., and Olson, E.N. (1988). Identification of upstream and intragenic regulatory elements that confer cell-type-restricted and differentiation-specific expression on the muscle creatine kinase gene. Mol Cell Biol *8*, 2896-2909.